NASA CONTRACTOR REPORT 165972

DESIGN, FABRICATION AND EVALUATION OF CHALCOGENIDE GLASS LUNEBURG LENSES FOR $LiNbO_3$ INTEGRATED OPTICAL DEVICES

V. E. WOOD, J. R. BUSCH, AND C. M. VERBER

BATTELLE COLUMBUS LABORATORIES
COLUMBUS, OH 43201

CONTRACT NAS1-16652
SEPTEMBER 1982

National Aeronautics and
Space Administration

Langley Research Center
Hampton, Virginia 23665

NASA CONTRACTOR REPORT 165972

DESIGN, FABRICATION AND EVALUATION OF CHALCOGENIDE GLASS LUNEBURG LENSES FOR $LiNbO_3$ INTEGRATED OPTICAL DEVICES

V. E. WOOD, J. R. BUSCH, AND C. M. VERBER

BATTELLE COLUMBUS LABORATORIES
COLUMBUS, OH 43201

CONTRACT NAS1-16652
SEPTEMBER 1982

National Aeronautics and
Space Administration

Langley Research Center
Hampton, Virginia 23665

TABLE OF CONTENTS

LIST OF FIGURES

SUMMARY

Optical-waveguide Luneburg lenses of arsenic trisulfide glass have been made and tested. The lenses are formed by thermal evaporation of As_2S_3 through suitably placed masks onto the surface of $LiNbO_3$:Ti indiffused waveguides. The lenses are designed for input apertures up to 1 cm and for speeds of f/5 or better. They are designed to focus the TM_0 guided mode of a beam of wavelength, external to the guide, of 633 nm. The refractive index of the As_2S_3 films and the changes induced in the refractive index by exposure to short-wavelength light have been measured. Some correlation between film thickness and optical properties was noted. The short-wavelength photosensitivity has been used to shorten the lens focal length from the as-deposited value. Lenses of rectangular shape, as viewed from above the guide, as well as conventional circular Luneburg lenses, have been made. Measurements made on the lenses include thickness profile, general optical quality, focal length, quality of focal spot, and effect of ultraviolet irradiation on optical properties. The best lenses had speeds of f/3 to f/2, and possessed good to very good focal properties--central spots within twice the diffraction-limited intensity width and primary sidelobes no more than 2 db above the diffraction-limited intensity--when stopped down to f/10 to f/5. Preliminary investigations of information-handling capacity of some lens were also carried out.

I. INTRODUCTION

This report describes the results of a one-year research program to develop chalcogenide-glass Luneburg lenses for use in $LiNbO_3$-based integrated optical devices. More specifically, we describe techniques developed in this program, and to some extent in parallel programs, for the design, fabrication, and testing of short-focal-length arsenic trisulfide Luneburg lenses on Ti-indiffused $LiNbO_3$ optical waveguides. As part of the program, techniques have been investigated for post-deposition modification of the optical properties of the lens by exposure to ultraviolet light. Two lenses, one modified as just described, have been prepared for delivery to the sponsor as specified in the contract.

In this report we first outline the theoretical and calculational procedures used to design the lenses, to design mask arrangements for production of these lenses by evaporation of the glass, and to assess the expected lens quality. Following this, we describe the experimental work of measuring the required material parameters and of fabricating and testing the lenses. In the present section we provide some background information and give a brief summary of our approach in order to motivate and to simplify the ensuing discussion.

A conventional Luneburg lens for use in planar integrated optics consists of a layer of high-refractive-index material deposited on a portion of an optical waveguide and radially symmetric about an axis through the center of the lens and perpendicular to the waveguide. Figure 1, in which this type of lens is illustrated along with the other principal types of waveguide lenses, should complement the verbal description. The effective refractive index of the guided mode is changed locally by an amount dependent on the thickness of the overlay at the point in question. The Luneburg lens is an example of a gradient-index lens, in which focusing occurs because of the difference in refractive index between adjacent rays. If the lens profile, thickness as a function of radius, is properly chosen, a perfect geometric focus can be obtained; that is, the lens will be diffraction-limited.

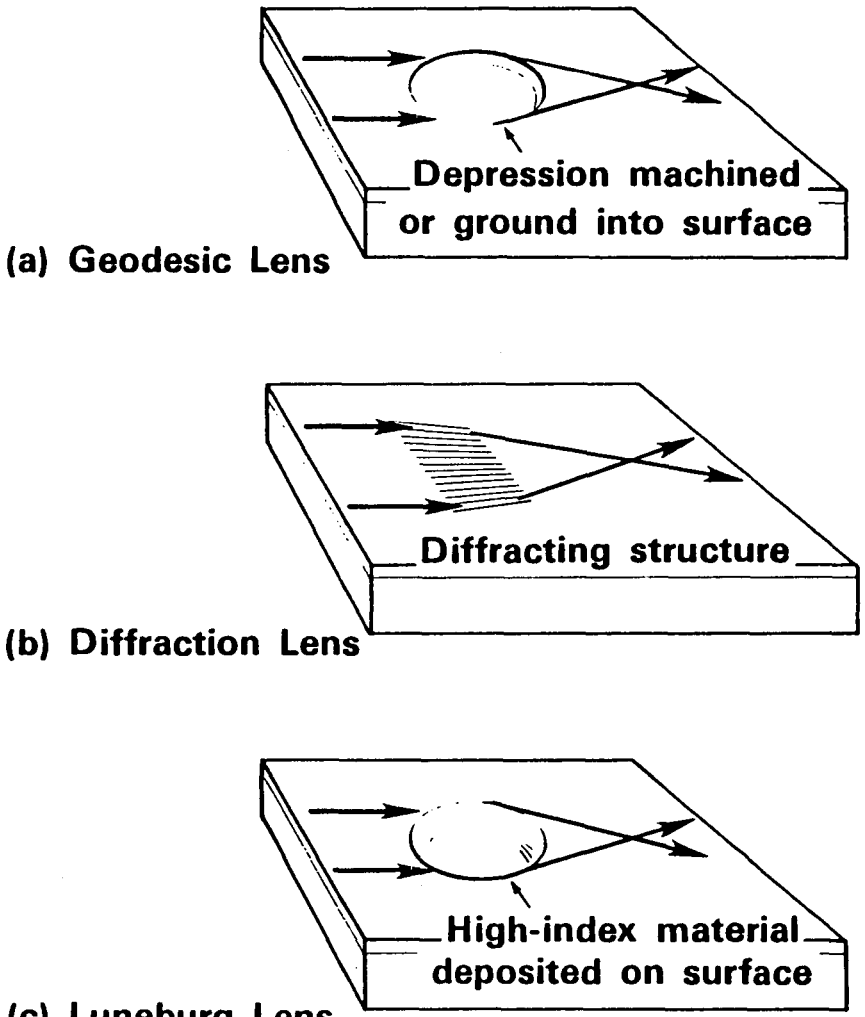

Fig. 1. Three types of short-focal-length lenses for use in integrated optics devices

The lens material should have a refractive index higher than that of the waveguide surface index, should not cause excessive absorption or scattering of the guided light, and should be easy to deposit on the waveguide surface. For lenses on $LiNbO_3$ waveguides, arsenic trisulfide (As_2S_3) glass is one of the few known materials to meet these criteria. As_2Se_3 and more complex chalcogenide glasses also have high refractive indices, but they have fundamental absorption edges more toward the infrared and cannot be used in the visible. ZnS and CdS have large energy gaps and high indices of refraction, and they can be deposited on $LiNbO_3$. These materials form polycrystalline films; obtaining films of good optical quality requires some care. Certain oxides, such as TiO_2, can in principle be used in conjunction with $LiNbO_3$ substrates, but in practice it is difficult to keep the oxygen content of the deposited films high enough to obtain a refractive index comparable with those of the crystal.

As_2S_3 may be deposited either by evaporation from a heated crucible or by rf sputtering. This glass has other useful properties as well. It may be removed without harm to the waveguide by dissolution in strong hydroxide solution, thus minimizing loss of expensive crystal substrates. It is also photosensitive, its refractive index increasing substantially (by more than 0.1) on exposure to blue or ultraviolet light. This phenomenon, or a similar permanent thermo-optic annealing effect, can be used for post-fabrication modification of the lens characteristics.

A brief survey of the development of Luneburg lenses and of As_2S_3 integrated-optics devices is provided in Appendix A.

Our present procedure for design and fabrication of Luneburg lenses comprises the following steps:

(1) An ideal Luneburg lens of the desired aperture and focal length, is designed, using standard procedures, for the waveguide mode and wavelength of interest. Design involves knowing something of the characteristics of the indiffused waveguide and selecting a target refractive index for the lens material, either the as-deposited index for the design wavelength or that expected after post-deposition modification.

(2) A mask arrangement suitable for producing a good approximation to the design lens profile is devised. In our work so far the lenses have been made by evaporation of the glass from a crucible through the mask apertures onto the waveguide; so the size of the crucible must be considered in the design. We have designed principally with only two masks, one to obtain the main part of the lens curvature and one to adjust the size and contour near the edge. The best mask positions and apertures are found approximately by a coarse optimization procedure and then refined by trial-and-error calculations.

(3) The lens is formed, as mentioned above, by evaporating powdered As_2S_3 glass from a quartz crucible onto the waveguide. The evaporation is carried out in a vacuum of around 1.0×10^{-5} torr. A piezoelectric thickness gauge is used to measure the amount of material deposited. The evaporation and masking configuration is sketched in Figure 2.

(4) If the lens is to undergo post-fabrication modification, it is subjected to a controlled exposure to ultraviolet light; otherwise it is protected from ultraviolet.

After a lens is made, it may be tested, optically and physically, in a variety of ways which we will describe in the appropriate place in the report.

II. THEORETICAL AND CALCULATIONAL WORK

A. Lens Design

The first step in lens design is, of course, selection of desired lens characteristics. Most of the lenses discussed in the present report have been designed for a focal length, within the waveguide, of 30 mm and

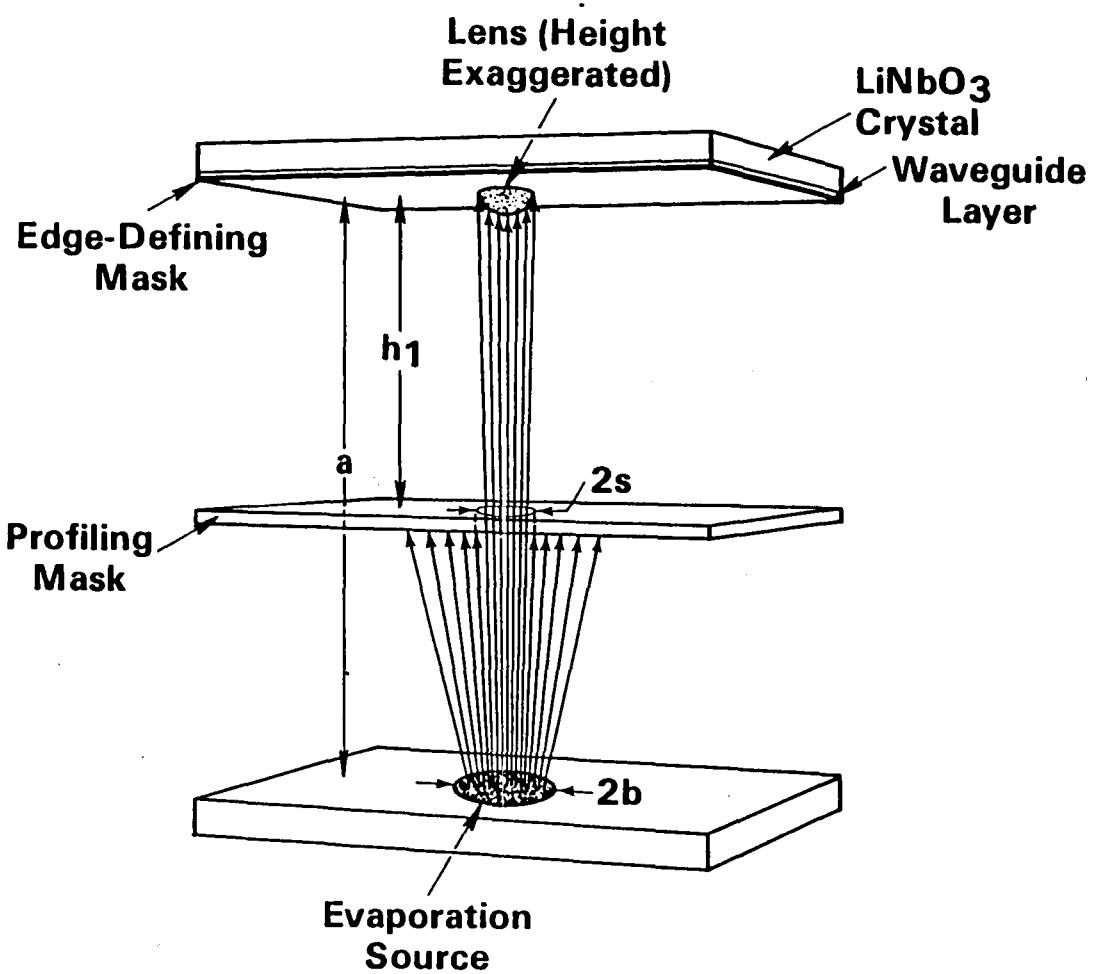

Fig. 2. Model of experimental arrangement for evaporation of As_2S_3 Luneburg lenses. Source is actually a crucible filled with powdered As_2S_3 glass.

an input aperture of 10 mm. They are intended to focus a TM_0 mode, of effective refractive index 2.288 in the waveguide region external to the lens. The designs are for light of free-space wavelength 633 nm. This set of characteristics provides a rather stringent test of design and fabrication capabilities.

With just the information given so far, we can determine the refractive index profile required for the lens by solving the Luneburg-Morgan integral equation:

$$\ln \frac{N(r)}{N_{ext}} = \frac{2}{\pi} \int_0^{(t - z)^{1/2}} \frac{\sin^{-1} (u^2 + z)}{(u^2 + 2z)^{1/2}} \, du. \qquad (1)$$

In this equation, N(r) is the mode index at radius r in the lens region, while N_{ext} is the mode index outside the lens. The parameter t is the reciprocal of twice the f/number of the lens, and z = tR, where $R = 2r\ N(r)/S\ Next$. A is the lens aperture. In the form presented here, the integral is easily evaluated to 5 decimal place accuracy by a single 16-point Gaussian quadrature. The design refractive index profile is shown in Figure 3.

To find the lens thickness profile corresponding to this refractive-index profile, we need the refractive-index profile of the diffused waveguide and the bulk refractive index of the lens material. We have taken the waveguide to have a Gaussian profile with a diffusion length of 2 μm, a surface index of 2.293, and a bulk index of 2.287. These values, which are not highly critical to the accuracy of the calculations, are typical of single-mode $LiNbO_3$:Ti waveguides for the polarization and wavelength conditions stated. Since the lens thickness varies slowly with radius, we can model the situation at a given radius as a uniform layer of lens material covering the inhomogeneous waveguide. We made a straightforward extension of the calculation method devised by Southwell (1977)* to this

* See the bibliography in Appendix A for citations of work referred to by author and year.

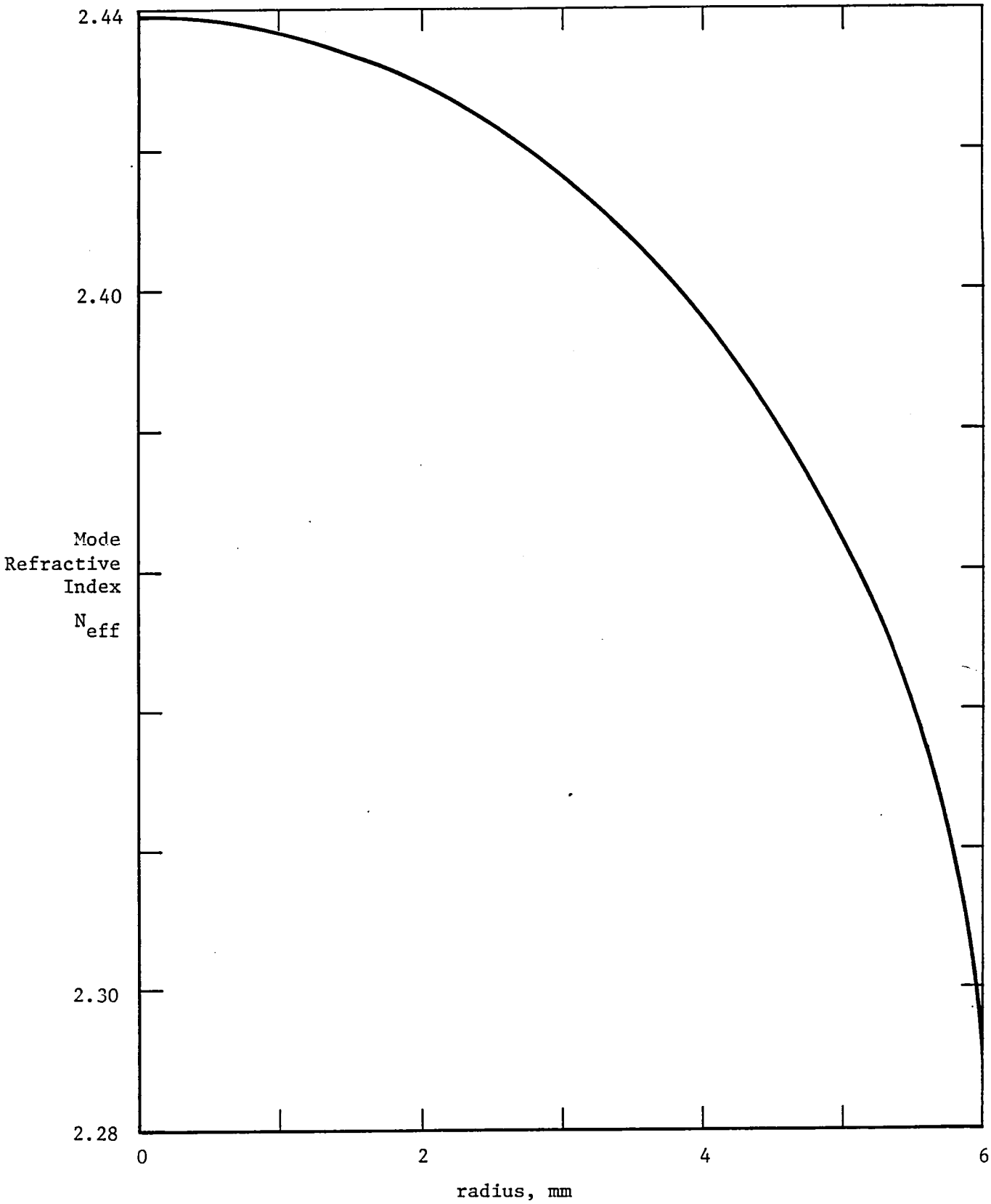

Figure 3. Required mode refractive index profile for f/3 Luneburg lens of 10 mm input aperture to focus TM_0 mode of $LiNbO_3$:Ti waveguide.

case. This analysis applies, strictly speaking, only to TE modes, except of course that index values appropriate to the TM_0 mode in the $LiNbO_3$ are inserted in the calculation. Subsequent work [see also Bryan et al. (1982)] has shown that while this is in most circumstances a fairly good approximation, it should be corrected for more accurate lens design and to allow better identification of sources of observed aberration; the required simple program modifications have not yet been made.

The refractive index at 633 nm of the As_2S_3 material was measured by methods described elsewhere in this report. We found the index of as-deposited As_2S_3 films to be about 2.445, with a fair amount of variation from sample to sample, which we presently believe may result mainly from variations in film stoichiometry with thickness. We made lens designs for film indices of 2.445, 2.46, and 2.48. The relative lens profiles, normalized to unity at the center of the lens, are shown in Fig. 4. The actual design central thicknesses are 1.69, 0.83, and 0.55 μm, respectively. This marked variation of required film thickness with assumed film index, and conversely of required film index with actual film thickness, brings out the importance of the post-fabrication index-modification capability.

B. Mask Design

Given the lens profile required for a particular focusing requirement, we need to determine apertures and positions of masks suitable for depositing a lens with this profile on the waveguide. We have found that fairly good approximations to profiles of interest can be obtained using only two thin masks.

The model for the evaporation system, and the system itself, have already been illustrated schematically in Figure 2.

The evaporation source is modeled as a uniform distribution over a circle of radius b of point sources, each emitting As_2S_3 molecules uniformly into the hemisphere above the source. The extent to which this simple model describes actual evaporation from a crucible has not been investigated

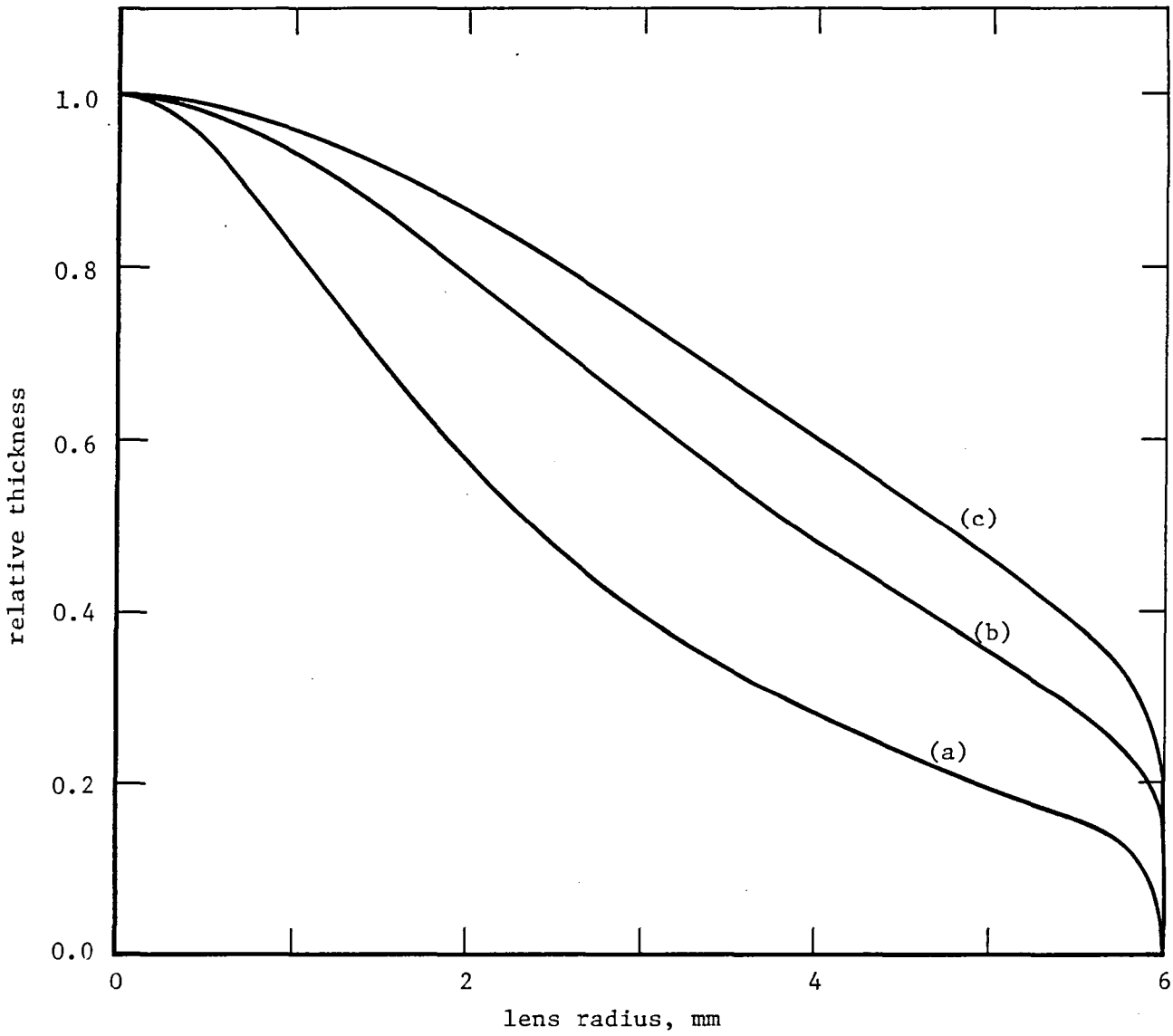

Fig. 4. Design profiles for As_2S_3 Luneburg lens on $LiNbO_3$ waveguide supporting a single TM mode for three values of lens refractive index n_f. (a) $n_f = 2.445$; (b) $n_f = 2.46$; (c) $n_f = 2.48$.

experimentally. It is possible that the geometric radius b' of the top of the crucible or the top of the melt differs from the effective source radius b that must be used in the model.

The lens-profiling mask is modeled as a simple circular hole in an infinitesimally thin sheet parallel to the waveguide surface. The distance h_1 of this sheet from the surface and the radius s of the hole are varied, first by a coarse least-squares procedure at five or six points and then by trial and error to optimize the fit to the desired profile. The fits are to a lens profile normalized to unity at the center; we rely on a separate measurement of the central thickness to obtain the proper lens thickness. To obtain a good fit near the edge of the lens, an additional mask very close to the substrate is used. It is positioned to reduce the lens thickness to zero at the desired aperture.

One cannot obtain lens profiles with regions of substantial upward curvature, such as shown in curve (a) of Figure 4, with only two masks. We tried nonetheless to make with two masks as good a fit as possible to this profile in order to test the adequacy of this simple arrangement. The expected attainable profile is compared to the design profile in Figure 5. The mask conditions to obtain this profile are as follows (dimensions in mm):

Mask	Distance below sample	Diameter
Source	100	18.3
Profiling	28	5.0
Edge-defining	0.5	11.9

Although the lens profile appears rather steep at the edge, lenses made according to this prescription did not produce any noticeable scattering into higher-order modes. Such scattering is readily observed since it produces overlapping output beams with two or more different focal lengths and consequently no single sharp focal plane. It is important that the overlay film be sufficiently tapered in thickness at the lens edges that these spurious modes in the lens region not be excited. Such modes occur when the required overlayer thickness is sufficient to allow higher modes in the underlying waveguide to exist. As the film thickness is increased,

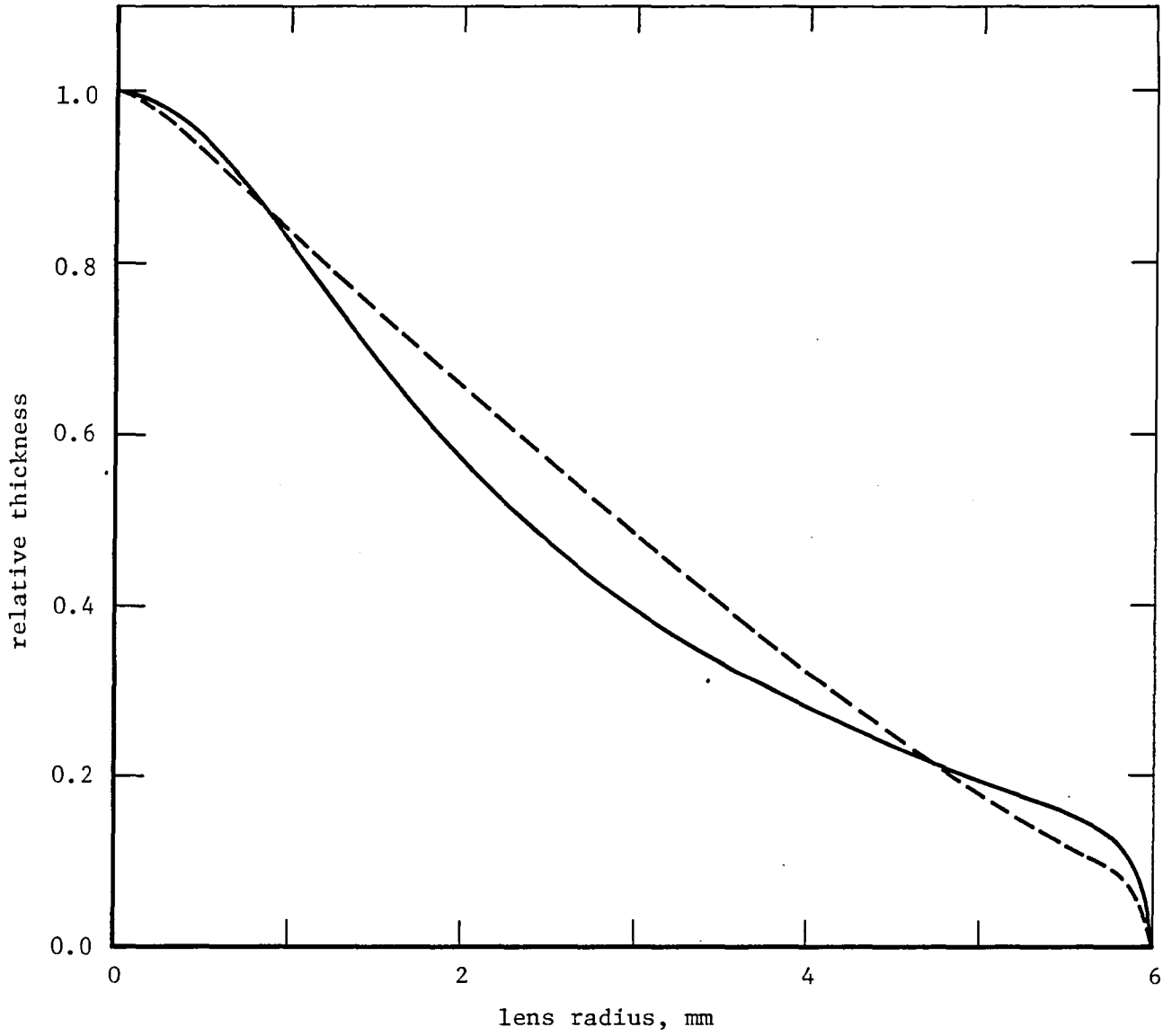

Fig. 5. Comparison of ideal profile of Luneburg lens (solid line) with possible actualization (dotted line) using two masks.

the single mode of the waveguide is slowly "pulled" up in effective index, until a point is reached when the index rapidly increases beyond the waveguide surface value, toward the bulk index of the film. As this rapid change is occurring, a new mode appears in the waveguide, a mode that was cut off for thinner films. This mode replaces the original single mode of the guide; its index rapidly increases to the vicinity of that of the original guided mode, where it remains until it too is finally pulled up into the film. This process continues, with new modes being pulled up into the guide from cutoff to replace lower modes that have been pulled into the film. As a result, there is, roughly speaking, almost always a mode present having an effective index very near that of the original waveguide. If the film thickness changes too rapidly at the edge, then in the region where the original mode is lifted into the film, strong coupling can occur between the incoming mode and the spurious mode lifted from the cutoff by the presence of the film. This coupling occurs because the effective index difference between the incoming mode and the spurious one is small and is changing more slowly than that between the incoming mode and its continuation in the film region. The result of such coupling is the appearance of multiple focused spots and increased apparent loss of transmission. The increased loss may not be too serious, but the transmission of the spurious modes through the lens is deleterious for most applications and can be disastrous for optical data processing.

III. EXPERIMENTAL WORK

A. Parameter Measurements

For accurate lens design and modification, and for calculation of lens properties, it is necessary to know several physical parameters of the lens material; consequently we have devoted considerable effort to measuring these parameters as determined under our evaporation conditions.

1. Lens Shape. As mentioned previously, the overall thickness of the lens is fixed by measuring the mass of material deposited on a piezoelectric thickness monitor mounted near the crystal but away from the masks. The mass/thickness ratio is determined by profilometer thickness measurements on test specimens. The profilometer, a Talysurf 4 manufactured by Taylor-Hobson, is also the principal instrument used to determine the lens profile. The stylus was not found to damage the arsenic trisulfide glass or the waveguide layer, and it is not too difficult to make a traverse through the thickest part of the lens. One difficulty with the Talysurf measurements is that the substrate near the lens was often found not to be flat; so it was necessary to make an extrapolation of substrate surface position beneath the lens in order to determine the lens thickness. It seems that the deposition of the lens may cause or enhance some warping of the substrate, especially as the effect seems to be more marked on thinner $LiNbO_3$ crystals. Departure of the substrate from planarity was not, however, observed to be sufficient to have any effect on the properties of the guided waves or of the lenses.

The profilometer work is complemented by interferometry. A Twyman-Green arrangement is used to provide interferograms of the lens shape; an example is shown in Figure 6. Both white-light and monochromatic illumination yield informative fringe patterns. Quantitative analysis of such fringe patterns has been limited to confirming approximate central thickness of the lens by fringe counting; but what the interferograms are particularly good for is detecting shape distortions resulting from misalignment of masks or from substrate imperfections.

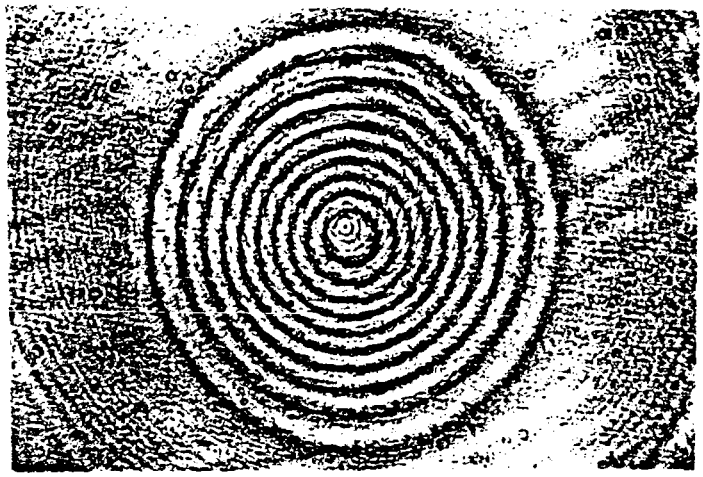

Fig. 6. Twyman-Green interferogram, made with 488 nm light, of As_2S_3 Luneburg lens, 1.2 μm thick at center and 1 cm in diameter, on $LiNbO_3$ substrate.

2. As_2S_3 refractive index. The refractive index at 633 nm of arsenic trisulfide films deposited according to our procedure has been measured by a prism deflection technique. Prisms of uniform thickness and apex angle 30° were deposited on $LiNbO_3$ waveguides through triangular masks held close to the guide. The prisms were oriented symmetrically with respect to the z-axis of the crystal and a 633 nm guided beam was coupled into the waveguide so it propagated along the x-axis of the y-cut crystal. After the beam was deflected by the overlay prism, it was end-fired out of the guide and its deflection was measured on a screen about a meter away. Because of the steep edges of the prisms, some of the light in the prism region was frequently scattered into, and subsequently back out of, higher-order modes, so there were usually 2 or 3 deflected beams corresponding to different modes in the prism region. For a 30° prism, the x-directed input beam exits at close to the expected angle of minimum deviation; it is difficult to find and to analyze the minimum deviation conditions accurately though, because of the variety of media through which the beam passes; so we analyzed the simpler situation of the initially x-propagating beam. From the observed deflection we calculate the mode indices in the prism region and from each mode index we calculate a value for the refractive index of the as-deposited overlay material. The unweighted average of 16 such determinations, measured on 6 prisms varying between 0.28 and 1.21 μm in thickness, was 2.445 ± 0.006. Two different substrates were used, and the modes observed were 6 TE_0, 6 TM_0, 3 TE_1 and 1 TM_1. The range of refractive indices found was 2.38 to 2.48, larger than desirable, but most of the values clustered well around the mean; consequently we adopt 2.445 as a provisional value in the design work. For the 7 TM modes the mean was also 2.445, while for the 6 TM_0 modes it was 2.447.

3. Ultraviolet-induced change in refractive index. The dynamic photoinduced index change was determined by measuring the change in the deflection of a guided TM_0 beam by an As_2S_3 prism as the prism was illuminated with an ultraviolet lamp. This prism again had apex angle 30°; it was 0.60 μm thick. The single-mode waveguide on which it was placed had polished end faces to improve the quality of the beam end-fired from the guide. The input coupling prism and the crystal were all enclosed in a plastic box

through which dry argon was flowed throughout the experiments. The ultraviolet illumination, strongest at 400 nm, impinged on the prism through the top of the box; the intensity of the 400 nm line at the sample, with the box cover in place, was 1.10 mW/cm^2. It was noticed that there was a small change in refraction by the prism between the time it was first made and when it was used in these experiments, although the sample had been kept in a desiccator and under yellow light. Backward extrapolation of the photoresponse dynamic curves indicated that this preliminary change in film index was equivalent to about 10 minutes extra exposure to the ultraviolet source. For exposure times up to about 3 hours, it was found that the refractive index of the As_2S_3 as measured by the deflection of the TM_0 mode could be expressed as

$$n = 2.5820 - 0.1295 \exp(-E/5.739), \tag{2}$$

where E is the total uv exposure (400 nm line) in J/cm^2. Such an expression is consistent with a model in which the rate of photoinduced index change is simply proportional to the remaining amount of unaltered material. For longer exposures up to 8 hours the film index increased above the saturation value indicated by Eq. (2) to 2.594. This effect is probably related to heating of the sample by the uv lamp; when the refractive-index changes were becoming small, long exposures (1 hour) were made between measurements. The prism region also supported a TM_1 mode; the dynamics of the index change measured using deflection of this mode were very similar to those with the TM_0 mode, but the apparent initial film index calculated for this mode was about 0.02 higher than that found using TM_0. After 6 hours exposure a TM_2 mode of even higher apparent index showed up. The observed index changes and model curves fitted to an equation of the type of (2) are shown in Figure 7. While heating of the sample seems to have a major influence on the values obtained at long times, the difference in the initial values should not go unremarked. We presently believe this difference may result from some dependence of film composition on evaporation time. Tanaka (1980) reports a fairly sharp peak in the ultraviolet photosensitivity at the stoichiometric composition As_2S_3. The refractive index of the as-deposited

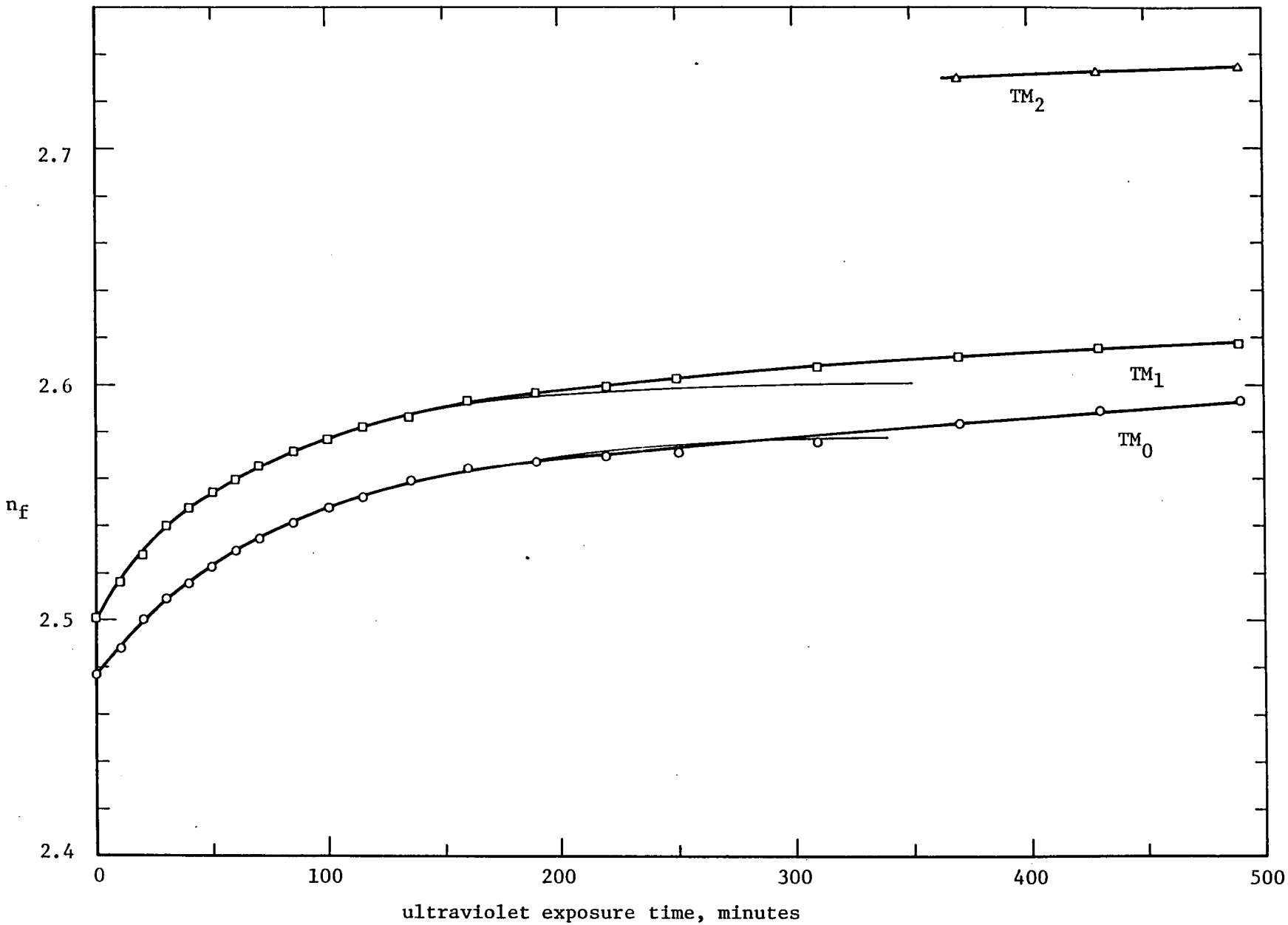

Figure 7. Apparent refractive index of As_2S_3 film prism as function of time of exposure to 1.1 mW/cm^2 of ultraviolet light, as determined by deflection of 3 different modes supported in prism region. Heavy lines connect data points; light lines are fits to data of the form $n_f = a - b \exp(-t/\tau)$.

film is also maximum near this composition; it falls off at higher sulfur concentrations but decreases little if at all, at more arsenic-rich compositions. It seems probable, therefore, that our films are near-stoichiometric when thin, but become somewhat sulfur-rich when thick. The vapor is believed to be sulfur-rich at all times during the evaporation; so the differences in film composition may be related to differences in condensation properties between the lithium niobate substrate and the chalcogenide glass itself. Higher-order guided modes, which have a mode index closer to that of the substrate than does the fundamental, yield higher film indices calculated on the basis of a uniform film because these modes are more effectively drawn into the high-index region near the surface. Several other experimental results, described elsewhere, tend to support this interpretation.

B. Lens Fabrication and Testing

In this section we provide a few details regarding our present waveguide and lens fabrication and testing procedures.

The optical waveguides were formed by evaporating 175 Å of titanium onto the surface of Y-cut $LiNbO_3$ crystals 1 to 3 mm thick and indiffusing this film at 1000 C for 2.5 h in an atmosphere of flowing oxygen which had been bubbled through water at 90 C. This procedure produces good quality waveguides supporting a single mode of each polarization at the design wavelength of 633 nm.

The lenses are made in a conventional bell-jar high-vacuum evaporation system, typically pumped down to a pressure of about 1.0×10^{-5} torr at the start of the evaporation. The source is 99.99% pure As_2S_3 fused glass which has been hand-ground in a porcelain mortar and pestle to a fine powder, approximately 325 mesh. The powder is evaporated from a quartz crucible held in a tungsten basket. The evaporation temperature is estimated to be in the 500 to 700 C range and the source-to-substrate distance is typically 100 mm. In our earlier experiments, the film deposition rate was around 20 nm/second. Since we considered that this

rapid evaporation rate might be a source of change in lens composition with thickness, we have more recently fabricated lenses using deposition rates of 1 to 2 nm/sec. While these more slowly deposited lenses are generally of better quality, there is so far no evidence that they are of more homogeneous composition. The masks are made of thin sheets of aluminum. The crystal substrate was not heated or cooled during the evaporation.

Post-fabrication modification of the lens refractive index was generally carried out with a more intense uv source than that used in the study of the dynamics of the index change. The intensity at the sample, measured at the dominant 400 nm line, was usually around 20 mW/cm^2. Reciprocity has been assumed in estimating index changes resulting from exposures at this level.

Our primary method for characterizing the optical quality of the Luneburg lenses has been the examination of the light distribution in the focal plane. The focal spot was scanned by coupling the beam transmitted through the lens out through a rutile prism and refocusing it with an f/2 imaging lens onto an optical multichannel analyzer. The experimental arrangement is shown in Figure 8. The OMA has 500 25 μm channels on 25 μm centers. The channels are long enough to collect substantially all the light diffracted or scattered in the direction perpendicular to the waveguide plane. In earlier work, we used a diode array or a fiber scanner to investigate the focal spot; in these cases an additional cylindrical lens was necessary to collect all the light. The OMA output can be displayed on an oscilloscope screen or recorded digitally.

In most cases the lenses focused outside the waveguide. To determine the focal length, we measured the length of the optical path in each medium--waveguide, output coupling prism if used, and air--from the lens center to the focal point, and converted the total distance to an equivalent distance inside the waveguide. The accuracy of such a procedure clearly cannot be very high; and our quoted focal lengths might easily be in error by $\pm$10%.

The information-handling capacity of the lenses has so far been investigated in only a preliminary way by placing a Ronchi ruling in the input beam and observing the relative intensity and width of the sidelobes

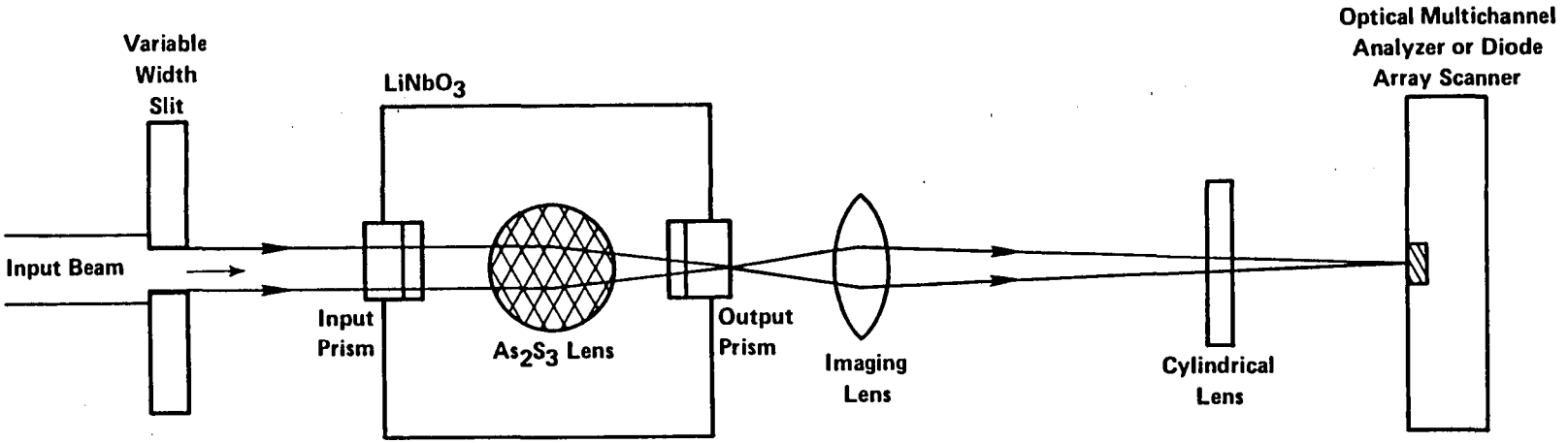

Fig. 8. Experimental arrangement for determining quality of lens focal spot. When the optical multichannel analyzer is used, the cylindrical lens is not needed.

generated in the output pattern. Only a few different rulings have been available. A better procedure seems to be to place some lenses on waveguides also containing broad-band surface-acoustic-wave transducers. These can be used to generate phase gratings of a range of spatial frequencies in the lens input plane, which should permit a determination of minimum and maximum resolvable spatial frequencies of the lens.

C. Summary of Some Experiments

Numerous lenses have been fabricated and tested. Some lenses showed a high degree of scattering of the guided light, so were not examined further. Usually the scattering appears to be related to the presence of trace amounts of diffusion-pump oil; thus, this source of scattering can presumably be eliminated by more frequent system maintenance. Some design, physical, and optical characteristics of several lenses are given in Table I. It will be noticed that the lens central thickness is frequently markedly different from the design thickness. In some cases this results from failure of the thickness monitor; in others it is intentional, to investigate the effect of varying lens thickness on the optical properties. The initial focal length does not vary as expected with the lens thickness. This may reflect changes in stoichiometry with lens thickness as previously discussed.

OMA scans of the lens focal spots have generally been made at reduced input aperture in order to be sure that all the light transmitted is captured by the relay lens and focused on the OMA detector. The diffraction patterns do not sharpen markedly at larger apertures, but we are at present not able to say how much of this effect, or noneffect, results from poorer quality of the lens near the periphery and how much from aperture effects in the light-collection system. The focal spot quality does not appear to vary in any marked or predictable way with lens thickness. The spot quality data may be compared with the ideal by using Eq. (1) of Appendix B. For 4 mm aperture and 25.6 mm focal length, the half power diffraction-limited spot size for the TM_0 mode at 633 nm is 1.6 μm.

TABLE I. PROPERTIES OF AS-PREPARED LENSES

Sample Number	Design: Aperture, mm useful/total	Design: Mask Arrangement	Measured: Thickness, μm	Measured: Focal Length, mm	Measured: Spot Size, μm	Measured: Sidelobe, height, dB	Comments
200A	6/8	(a)	0.36	42.8	8.32	-9.4	-
198A	6/8	(a)	0.30	168.7	-	-	-
199	6/8	(a)	-	56.5	-	-	
200B	6/8	(a)	-	125.2	-	-	Samples 200 & 198 were reused.
198B	6/8	(a)	-	273.0	-	-	-
124	6/8	(a)	-	43.0	-	-	
HP-6	10/12	(b)	0.68	15.0(TE_o)			Subsequently annealed at 190 C for 30min. in flowing Argon. Focal length reduced to 15.0 mm (TM_o)
				28.7(TM_o)	2.9	-7	
250	10/12	(b)	0.96	22.2	-	-	As deposited, thicker lenses have longer focal lengths
166	10/12	(b)	1.20	26.7	-	-	
226A	10/12	(b)	1.20	31.3	-	-	
206	10/12	(b)	1.46	31.3	-	-	-
253	10/12	(b)	0.80	17.6(TE_o)	5.8	-11.1	
		(b)		22.2(TM_o)	5.5	-6.2	
226B	10/12	(b)	0.70	17.6(TE_o)			Sample #226 was reused. TE_o focal spot was also sharp, but was not scanned
				24.5(TM_o)	2.28	-11.2	
W-1	10/13	(c)	0.56	92.3	7.3	-4.3	Rectangular (4x13 mm)
W-2	10/13	(c)	0.89	115.2	8.84	-4.8	Rectangular

*(a) Source to $LiNbO_3$ 100 mm; profiling mask aperture 4.1 mm, position 23.5 mm below waveguide; edge-defining mask aperture 7.8 mm, position 0.75 mm below waveguide.

(b) For mask arrangement see p. 11.

(c) For mask arrangement see p. 44.

For the ideal lens the first sidelobes should be 13.3 dB down in intensity from the central peak. The two numbers given, focal spot size and first sidelobe intensity, do not fully characterize the lens quality, of course, even at fixed input aperture. It should also be borne in mind that the input beam is a truncated Gaussian rather than an ideal plane wave. In Table II we summarize effects of short wavelength light, from a variety of sources, on the optical properties of a number of lenses. While ultraviolet exposure reduces the focal length markedly by increasing the refractive index of the lens material, it does not generally lead to marked deterioration in apparent focal spot quality. After long exposure the fraction of light in the sidelobes tends to increase, though; and sometimes, as in lens W-2, it becomes quite large.

Further lens testing was done by placing Ronchi rulings in the input beam and examining the resulting focal pattern. The experimental setup is sketched in Figure 9. The light passing through the lens was coupled out of the waveguide and the focal plane intensity imaged at a magnification of 44. Photographs of such re-imaged focal planes for lens 226B are shown in Figure 10. The principal diffraction peaks from a grating of 2.36 lines/mm (60 lines/inch) are imaged adequately, and those from a grating of 7.87 lines/mm (200 lines/inch) are well-separated. The positions of these peaks were measured on the original photographs; they occurred where expected. For an ideal Ronchi ruling illuminated by a plane wave, the second-order principal diffraction peak should be absent. Traces of this peak are apparent in both photographs, although with the coarser ruling it is evident that the third-order peaks are stronger. Further experiments to characterize more fully the spatial information handling capacity of the lenses are planned.

TABLE II. EFFECTS OF EXPOSURE ON LENS PROPERTIES

Sample Number	Exposure-Source	Focal Length, mm	Spotsize, - At Aperture, μm	mm	Side lobe Height, dB	Comments
200A	0	42.8	8.32	4	-9.4	-
	0.25J-25W bulb[a]	24.5	4.87	4	-11.1	-
198A	0	168.7	-	-	-	-
	0.5J-25W bulb	26.7	6.32	4	-13.0	-
199	0	56.5	-	-	-	Exposure measured with broadband laser power meter
	0.60J-Argon Laser[b]	45.1	-	-	-	
	2.4J-Argon Laser	38.2	-	-	-	
200B	0	125.2				Exposure measured with broadband laser power meter
	60mJ-Blacklight[c]	104.6	-	-	-	
	90mJ-Blacklight	93.2				
	150mJ-Blacklight	81.7				
	540mJ-Blacklight	54.2				
198	0	273.0	-	-	-	
	0.13J-25W Bulb	103.0				
	0.20J-25W Bulb	63.0				
	0.46J-25W Bulb	43.0				
124	0	43.0				
	2.16J-Flood Lamp[d]	38.0				
	14.4J-Flood Lamp	33.0				

TABLE II. (Continued)

Sample Number	Exposure-Source	Focal Length, mm	Spot Size - At Aperture, μm	mm	Sidelobe Height, dB	Comments
250	0	22.2	-	-	-	-
	61J-UV Lamp[e]	17.6	-	-	-	-
	122J-UV Lamp	13.0	-	-	-	-
166	0	26.7	-	-	-	-
	61J-UV Lamp	22.2	-	-	-	-
	122J-UV Lamp	17.6 (TM_0)	2.93 μm	$4(TM_0)$	$-13.6(TM_0)$	Very good quality lens
		17.6 (TE_0)				
226A	0	31.3	-	-	-	-
	61J -UV Lamp	22.2				Both samples 226A and 206 did not focus very sharply as deposited, but did after UV exposure.
	122J-UV Lamp	17.6	-	-	-	
206	0	31.3	-	-	-	
	61J-UV Lamp	26.7				
	122J-UV Lamp	22.2				
W-1	0	92.3	7.3	3	-4.3	Rectangular
	1.98J-UV Lamp	92.3	11.34	3	-6.3	Spot size increased, side lobes decreased
	32.6J-UV Lamp	56.6	5.35	3	-5.1	Optimum exposure
	93.8J-UV Lamp	51.0	5.91	3	-3.9	-
W-2	0	115.2	8.84	3	-4.8	Rectangular
	30.6-UV Lamp	92.3	9.18	3	-5.3	Spotsize increased, side lobes decreased
	91.8J-UV Lamp	80.8	7.18	3	-3.1	Spotsize decreased, but side lobes increased
	153.0J-UV Lamp	69.4	6.95	3	-2.7	

TABLE II. (Continued)

(a) 25W incadescent bulb, measured at 400 nm, ± 50 nm bandwidth.

(b) 488 nm line of Ar-ion laser

(c) Low intensity long-wavelength-UV blacklight.

(d) 125W floodlamp, measured at 400 nm.

(e) Ultraviolet lamp, measured at 400 nm.

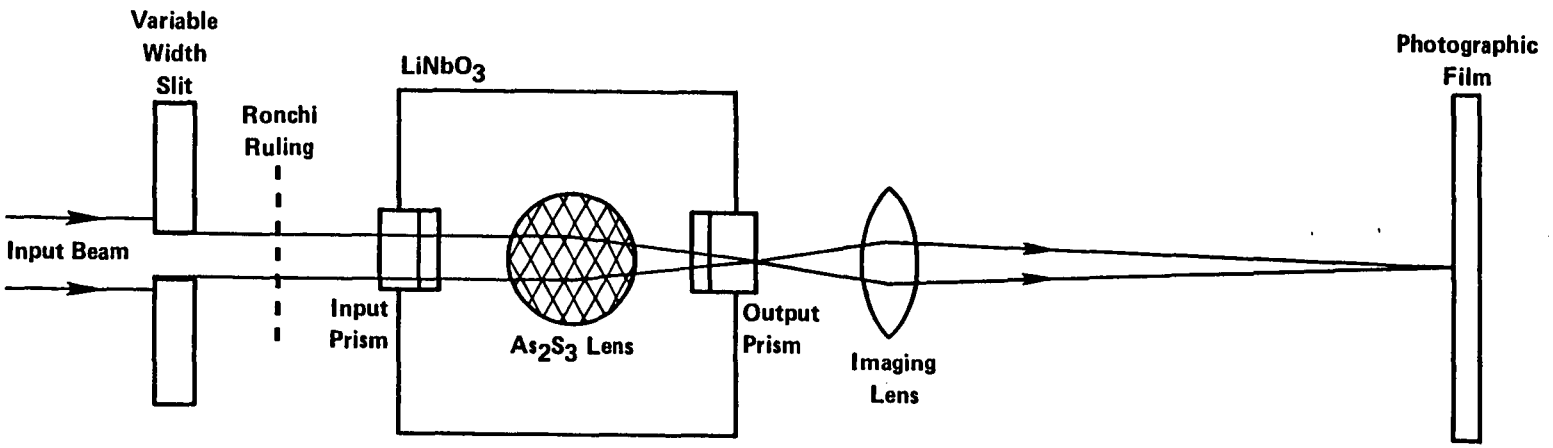

Fig. 9. Experimental arrangement for investigation of spatial-frequency response of lenses using Ronchi rulings. The input beam must be well collimated.

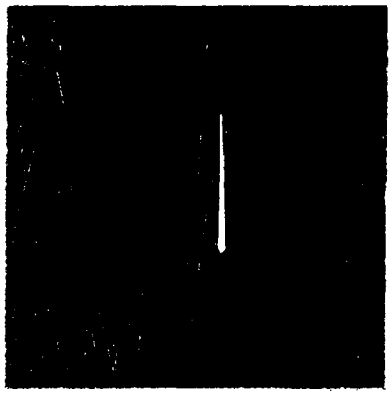

no ruling

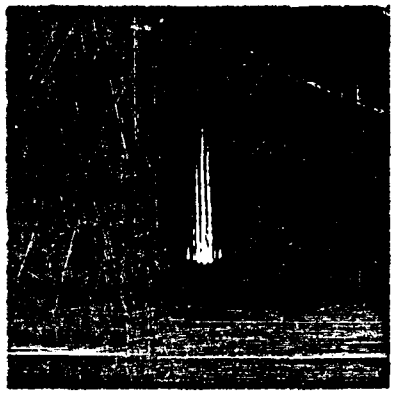

2.36 lines/mm
Ronchi ruling

7.87 lines/mm
Ronchi ruling

Fig. 10. Focal plane images of Ronchi rulings placed in input beam to lens 226B

IV. OTHER ACTIVITIES

A. Rectangular Lens

Integrated-optics Luneburg lenses as conventionally described have a circular outline as viewed from above the waveguide. Other shapes are not prohibited, though; in particular, W. H. Southwell had described Luneburg-type lenses of rectangular outline which promise considerable savings in space on the waveguide when a very large field of view is not required. We have made, by evaporating As_2S_3 onto $LiNbO_3$:Ti waveguides, some lenses of this type and measured their optical characteristics. Our work is described in a paper to be submitted for publication shortly. A preliminary version of this paper is included as Appendix B.

B. Presentations and Publications

Talks describing some of the work on this program were given by J. R. Busch at the NASA Conference on Optical Information Processing for Aerospace Applications, August 1981, and by V. E. Wood at the Optical Society of America Annual Meeting, October 1981. Information on publications resulting from these talks, and on the planned rectangular lens paper, is summarized in Appendix C.

V. CONCLUSIONS

This program has been successful in showing that short-focal-length lenses of good quality can be reliably fabricated by depositing arsenic trisulfide through suitable masks onto $LiNbO_3$:Ti waveguides. A number of incompletely resolved questions remain, however, and several process improvements will be required if near diffraction-limited performance is to be reproducibly achieved. Among the areas where further work is desirable are: improved control of composition and homogeneity of the lens material, minor improvements to lens design programs, more general mask design, ray-tracing studies of fabrication tolerances, and refinement of photosensitivity data.

APPENDIX A

HISTORICAL SKETCH

APPENDIX A

HISTORICAL SKETCH

Lenses of the type associated with the name of R. K. Luneburg were first described by him in lectures of 1944. His discussion covers more general lenses than the sphere with $n^2(r) = 2 - r^2$ mentioned by Born and Wolf. Generalizations of Luneburg's ideas were made by a number of workers; papers by Kunz (1954), Toraldo di Francia (1955), and Morgan (1958, 1959) summarize much of this early work, which was mostly directed toward microwave applications. The Luneburg lens was introduced into integrated optics by Zernike (1974), who deposited Nb_2O_5 lenses through a tapered mask onto glass waveguides. Design principles for integrated-optics Luneburg lenses on uniform waveguide layers were given by Southwell (1977a, b).

Yao and Anderson (1978, 1979) demonstrated diffraction-limited f/5 Luneburg lenses made by sputtering Ta_2O_5 onto uniform glass waveguides.

Hatakoshi and co-workers (1979) described f/2 lenses formed by evaporation of ZnS onto glass waveguides. Both Yao et al and Hatakoshi et al discuss briefly the design of profiling masks. Their lenses were designed to focus a TE mode, to which Southwell's analysis applied. Bryan et al (1982) adapted this work to the design and fabrication of TM-mode Luneburg lenses of Ta_2O_5 on glass waveguides. Luneburg lenses on inhomogeneous waveguides, such as are formed by difffusion or by ion exchange, were first described by Busch et al (1981), who also discussed the modifications to Southwell's design procedure necessary

to treat this situation. Recent topics of interest include development of more tolerant designs for given depth of focus (Colombini, 1981); the possibility of ion-implanted Luneburg lenses (Sochacki, 1982); and lenses deviating from circular symmetry (Southwell, 1981, 1982).

The development of As_2S_3 glass has been reviewed by Frerichs (1953). As_2S_3 films were first considered for use in integrated optics because of their good acoustooptic properties (Dixon, 1967; Ohmachi, 1973), although they display high acoustic attenuation. Young (1971) was among the first to prepare evaporated glassy As_2S_3 films of good optical quality. The use of such films for waveguiding and for other integrated-optics applications was promoted by Klein (1974). The photo-induced changes in refractive index were described by Keneman (1971) and by Ohmachi and Igo (1972). Related changes in optical absorption were first noted by Kostyshin et al (1966) and were described more completely by Berkes et al (1971) and by Igo and Toyoshima (1972). Chemical changes, revealed by etching-rate experiments, related to the optical changes were found by Keneman (1974). Films made by rf sputtering were first reported by Watts et al (1974). The dependence of the photo-induced changes on glass composition has been extensively studied by Tanaka and co-workers; a recent paper (Tanaka, 1980) contains references to earlier work. A number of models have been proposed to explain the photoeffects at an atomic or molecular level; papers by Halpern (1976), Bishop and Taylor (1979), and Biegelsen and Street (1980) provide physical descriptions of several of these models. Among the many integrated-optical devices made using As_2S_3 films, we mention only a multiplexer (Handa et al, 1980) and a light-controlled switch (Tanaka and Odajima, 1981). The remarkable

glass-forming tendency of As_2S_3 is discussed by Phillips (1982).

Many additional works might be cited; this brief survey has dealt principally with those bearing on the present study. We have also included a number of references which survey other work and provide further references. A bibliography of works we have referred to follows.

Bibiliography

Berkes et al, 1971 — J. S. Berkes, S. W. Ing, Jr., and W. J. Hillegas, "Photodecomposition of amorphous As_2Se_3 and As_2S_3." J. Appl. Phys. 42, 4908-4916 (1971).

Biegelsen and Street, 1980 — D. K. Biegelsen and R. A. Street, "Photoinduced defects in chalcogenide glasses." Phys. Rev. Lett. 44, 803-806 (1980).

Bishop and Taylor, 1979 — S. G. Bishop and P. C. Taylor, "Iron impurities as non-radiative recombination centres in chalcogenide glasses." Phil. Mag. B 40, 483-495 (1979).

Born and Wolf, 1975 — M. Born and E. Wolf, Principles of Optics, 5th ed., p. 147 (Pergamon Press, Oxford, U. K., 1975).

Bryan et al, 1982 — D. A. Bryan, C. R. Chubb, J. K. Powers, H. E. Tomaschke, W. R. Reed and E. A. Dalke, "Development of a tantalum pentoxide Luneburg lens." Proc. SPIE 321, to be published (1982).

Busch et al, 1981 — J. R. Busch, V. E. Wood, R. P. Kenan and C. M. Verber, "Evaporated As_2S_3 Luneburg lenses for $LiNbO_3$:Ti optical waveguides." Optical Information Processing for Aerospace Applications, NASA Conference Publication 2207, p. 251-261 (NASA Sci. and Techn.

Info. Branch, 1981).

Colombini, 1981 — E. Colombini, "Design of thin-film Luneburg lenses for maximum focal length control." Appl. Opt. 20, 3589-3593, (1981).

Dixon, 1967 — R. W. Dixon, "Photoelastic properties of selected materials and their relevance for applications to acoustic light modulators and scanners." J. Appl. Phys. 38, 5149-5153 (1967).

Frerichs, 1953 — R. Frerichs, "New optical glasses with good transparency in the infrared." J. Opt. Soc. Amer. 43, 1153-1157 (1953).

Halpern, 1976 — V. Halpern, "Localized electron states in the arsenic chalcogenides." Phil. Mag. 34, 331-335 (1976).

Handa et al, 1980 — Y. Handa, T. Suhara, H. Nishihara and J. Koyama, "Integrated grating circuit for guided-beam multiple division fabricated by electron-beam direct writing." Optics Lett. 5, 309-311 (1980).

Hatakoshi et al, 1979 — G. Hatakoshi, H. Inoue, K. Naito, S. Umegaki and S. Tanaka, "Optical waveguide lenses." Optica Acta 26, 961-968 (1979).

Igo and Toyoshima, 1972 — T. Igo and Y. Toyoshima, "Optically induced reversible change in amorphous semiconductors." Japan. J. Appl. Phys. 11, 117-118 (1972).

Keneman, 1971 — S. A. Keneman, "Hologram storage in arsenic trisulfide thin films." Appl. Phys. Lett. 19, 205-207 (1971).

Keneman, 1974 — S. A. Keneman, "Surface relief holograms in evaporated arsenic trisulfide films." Thin Solid Films 21, 281-285 (1974).

Klein, 1974 — R. M. Klein, "Chalcogenide glasses as passive thin film structures for integrated optics." J. Electron. Materials 3, 79-99 (1974).

Kostyshin et al, 1966 — M. T. Kostyshin, E. V. Mikhailovskaya and P. F. Romanenko, "Photographic sensitivity effect in thin semiconducting films on metal substrates." Sov. Phys.--Solid State 8, 451-452 (1966).

Kunz, 1954 — K. S. Kunz, "Propagation of microwaves between a parallel pair of doubly curved conducting surfaces." J. Appl. Phys. 25, 642-653 (1954).

Luneburg, 1944 — R. K. Luneburg, Mathematical Theory of Optics, p. 208-213 (Brown Univ., Providence RI, 1944).

Morgan, 1958 — S. P. Morgan, "General solution of the Luneburg lens problem." J. Appl. Phys. 29, 1358-1368 (1958).

Morgan, 1959 — S. P. Morgan, "Generalizations of spherically symmetric lenses." IRE Trans. Antenn. Propg. AP-7, 342-345 (1959).

Ohmachi and Igo, 1972 — Y. Ohmachi and T. Igo, "Laser-induced refractive-index change in As-S-Ge glasses." Appl. Phys. Lett. 20, 506-508 (1972).

Ohmachi, 1973 — Y. Ohmachi, "Acousto-optical light diffraction in thin films." J. Appl. Phys. 44, 3928-3933 (1973).

Phillips, 1982 — J. C. Phillips, "The physics of glass." Physics Today 35, #2, 27-33 (1982).

Sochacki, 1982 — J. Sochacki, "Proposal for an alternate technology for waveguide Luneburg lenses." Opt. Commun. 41, 13-16 (1982).

Southwell, 1977a — W. H. Southwell, "Inhomogeneous optical waveguide lens analysis." J. Opt. Soc. Amer. 67, 1004-1009 (1977).

Southwell, 1977b — W. H. Southwell, "Index profiles for generalized Luneburg lenses and their use in planar optical waveguides." J. Opt. Soc. Amer. 67, 1010-1014 (1977).

Southwell, 1981 — W. H. Southwell, "Planar optical waveguide lens design." J. Opt. Soc. Amer. 71, 1581 (1981). (Abstract)

Southwell, 1982 — W. H. Southwell, "Planar optical waveguide lens design." Appl. Opt. 21, to be published (1982).

Tanaka, 1980 — K. Tanaka, "Optical properties and photoinduced changes in amorphous As-S films." Thin Solid Films 66, 271-279 (1980).

Tanaka and Odajima, 1981 — K. Tanaka and A. Odajima, "Photo-optical switching devices by amorphous As2S3 waveguides." Appl. Phys. Lett. 38, 481-482 (1981).

Toraldo di Francia, 1955 — G. Toraldo di Francia, "A family of perfect configuration lenses of revolution." Optica Acta 1, 157-163 (1955).

Watts et al, 1974 — R. K. Watts, M. de Wit and W. C. Holton, "Nonoxide chalcogenide glass films for integrated optics." Appl. Opt. 13, 2329-2332 (1974).

Yao and Anderson, 1978 — S. K. Yao and D. B. Anderson, "Shadow sputtered diffraction-limited waveguide Luneburg lenses." Appl. Phys. Lett. 33, 307-309 (1978).

Yao et al, 1979 — S. K. Yao, D. B. Anderson, R. R. August, B. R. Youmans and C. M. Oania, "Guided-wave optical thin-film Luneburg lenses: fabrication technique and properties." Appl. Opt. 18, 4067-4079 (1979).

Young, 1971 — P. A. Young, "Optical properties of vitreous arsenic trisulphide." J. Phys. C 4, 93-106 (1971).

Zernike, 1974 — F. Zernike, "Luneburg lens for optical waveguide use." Opt. Commun. 12, 379-381 (1974).

APPENDIX B

PRELIMINARY VERSION OF PAPER

RECTANGULAR LUNEBURG-TYPE LENSES FOR INTEGRATED OPTICS

APPENDIX B

Preliminary version of paper

RECTANGULAR LUNEBURG-TYPE LENSES FOR INTEGRATED OPTICS

Van E. Wood and James R. Busch
Battelle Columbus Laboratories, 505 King Avenue, Columbus, Ohio 43201

Duncan T. Moore and Ben Woolley
Institute of Optics, University of Rochester, Rochester, New York 14627

W. H. Southwell
Rocketdyne Division, Rockwell International, Canoga Park, California 91304

Abstract

Compact Luneburg-type lenses of rectangular outline as viewed from above have been made by thermal evaporation of As_2S_3 glass onto single-mode $LiNbO_3$:Ti waveguides through suitably shaped masks and subsequent exposure of the glass to ultraviolet light. The best lenses had speeds of f/5.5 at an aperture of 10 mm and focal spots at reduced aperture about 1.2 times the diffraction-limited size. These lenses have a field of view of at least 25 degrees inside the waveguide.

Among the types of lenses which may be used in integrated optics devices, Luneburg lenses possess advantages of ease of fabrication and freedom from aberrations. Diffraction-limited Luneburg lenses have been made[1] by sputtering Ta_2O_5 onto glass waveguides; lenses of fairly good quality made by evaporation of As_2S_3 glass onto Ti-indiffused $LiNbO_3$ waveguides have also been described[2]. Conventional Luneburg lenses[3,4] are circular in outline as viewed from above the waveguide and thus have the additional advantage of a 360 degree field of view. If an unlimited field of view is not required, lenses of different outline are conceivable; in particular, it has recently been shown[5] that diffraction-limited Luneburg-type lenses with a rectangular outline can be designed. These lenses offer considerable savings in space, particularly important on single-crystal substrates. They may also offer advantages over conventional Luneburg lenses of wider fabrication tolerances and reduced probablility of scattering into the higher-order guided modes which are usually present in the lens region. In the present paper, we describe Luneburg-type lenses of approximately rectangular outline formed

by thermal evaporation of As_2S_3 through suitable masks onto single-mode $LiNbO_3$ waveguides.

The optical waveguides were formed by evaporating 175 Å of titanium onto the surface of a Y-cut $LiNbO_3$ crystal 3 mm thick and indiffusing this film at 1000 C for 2.5 h in an atmosphere of flowing oxygen which had been bubbled through water at 90 C. This procedure produces good quality waveguides supporting a single mode of each polarization at a wavelength (in air) of 633 nm; Nomarski micrographs show a surface free of "orange peel" or other indications of residual oxides of titanium or other metals.

No formal design procedures have been followed so far in making the lenses; rather we have drawn on experience with conventional circular-outline Luneburg lenses and also have relied on trial and error; unsatisfactory lenses are easily removed without damage to the waveguide by dissolving them in KOH. The lenses are formed by evaporating powdered As_2S_3 glass from a crucible of circular cross-section, 18.3 mm in diameter at its mouth and 110 mm from the waveguide surface. The crystal substrate was not heated during the evaporation. The lenses were configured using one circular-aperture and one rectangular-aperture mask. For example, one lens was made by placing the circular mask, which had an aperture of diameter 5.0 mm, 38.0 mm below the crystal; and the rectangular mask, which had an aperture 2 mm by 11 mm, 10.0 mm from the crystal. After the deposition, the lens was illuminated with an ultraviolet lamp to increase its refractive index. The total exposure, measured at the dominant 400 nm line of the lamp, was 33 J/cm^2. According to prism-deflection experiments we have carried out, this exposure should increase the glass refractive index to about 2.58. A Twyman-Green interferogram of this lens is shown in Fig. 1. The large fringes visible on the periphery of the lens arise from flexing or bowing of the $LiNbO_3$ substrate. The lens is 13 mm wide and 4 mm thick. Talysurfs of the two principal directions showed that it is about 560 nm high at the center; this measurement was confirmed by fringe counting on the interferogram.

The focusing properties of a similar lens for a 9 mm wide truncated Gaussian input beam propagating in the TE_0 mode are shown in Fig. 2. The light source was the 633 nm line of a He-Ne laser. No effects of scattering into higher-order guided modes in the lens region were noted. The measured focal length is 35 mm for the normal-incidence beam; so the lens speed is f/3.9 for the aperture used or f/2.9 for the full lens width (12 mm). The useful field of view of the lens, as judged by the range of input directions which yielded an apparent sharp focus for an input beam 9 mm wide, is at least 25 degrees, as measured inside the waveguide.

The lens shown in Fig. 1 initially focused the TM_0 mode at 92 mm as measured in the waveguide. After the 33 J/cm^2 uv exposure, the focal length was reduced to 55 mm. The focal spot of the lens was scanned by coupling the transmitted beam out through a rutile prism and refocusing it onto an optical multichannel analyzer. The aperture was reduced to 3 mm in making the focal scans in order to ensure that all the light was captured by the relay lens. Traces of the OMA output are shown in Fig. 3. For a one-dimensional lens, the half-power diffraction-limited spot size is given by

$$S = 0.8859\ (\lambda_0\ f)/(n_{ext}\ w); \qquad (1)$$

where λ_0 is the external wavelength of the light used, n_{ext} is the mode index outside the lens region, taken as 2.289, f is the lens focal length as measured in the waveguide, and w is the input aperture. For the conditions stated, the expected minimum spot size after the uv exposure is 4.5 μm. The measured value is 5.4 μm; so at this aperture the lens is about 1.2 times diffraction-limited. As the data in Fig. 3 show, before exposure to uv light, the focal spot was symmetric with most of the energy confined to the central peak, whose half-power width was 11.3 μm, 1.5 times the diffraction-limited value, the first sidelobes being 6.7 dB down. After exposure to 33 J/cm^2 of uv light the central spot width decreased to 5.4 μm, but some of the symmetry was lost and more energy was spread into the first sidelobes (now 5.0 dB down) and into the wings of the distribution. Further uv exposure shortened the focal length to 51 mm but led to deterioration in the spot quality.

In summary, compact, fast, Luneburg-type lenses of good quality have been made by evaporation of As_2S_3 onto $LiNbO_3$:Ti waveguides through a rectangular mask, followed by exposure to ultraviolet light. There is room for improvement, though, in the focal-spot quality.

We wish to thank Mark Parmenter, Richard Kenan, Carl Verber, and Philip Jenkins for their contributions to this research. Work at Battelle was supported by NASA-Langley Research Center and also benefited from support of parallel work by Harry Diamond Laboratories, U. S. Department of the Army.

References

1. S. K. Yao and D. B. Anderson, "Shadow sputtered diffraction-limited waveguide lenses," Appl. Phys. Lett. 33, 307 (1978).
2. James R. Busch, Van E. Wood, Richard P. Kenan, and Carl M. Verber, "Evaporated As_2S_3 Luneburg lenses for $LiNbO_3$:Ti optical waveguides," Optical Information Processing for Aerospace Applications, NASA Conference Publication 2207 (NASA Scientific and Technical Information Branch, 1981), p. 251. C. M. Verber, J. R. Busch, and Van E. Wood, "As_2S_3 Luneburg Lenses on $LiNbO_3$ waveguides," J. Opt. Soc. Amer. 71, 1559 (1981) (abstract).
3. R. K. Luneburg, Mathematical Theory Of Optics (Brown University, Providence, RI, 1944), Sec. 29.
4. W. H. Southwell, "Index profiles for generalized Luneburg lenses and their use in planar optical waveguides," J. Opt. Soc. Amer. 67, 1010 (1977).
5. W. H. Southwell, "Planar optical waveguide lens design," Appl. Opt. 21, 1985 (1982).

Figure Captions

Fig. 1. Twyman-Green interferogram of As_2S_3 Luneburg lens on $LiNbO_3$ substrate. The light source is the 488 nm line of an Ar laser, polarized predominantly vertically. The small interference features along the ridge probably result from diffraction due to the steep front and back edges of the lens.

Fig. 2. Focusing characteristics of a lens similar to the lens of Fig. 1. The transmitted beam was rendered visible by a white spray paint layer. (a) Normally incident beam, 9 mm wide. (b) Beam incident at 6.4 degrees from normal incidence, again 9 mm wide. The light source is the 633 nm line of a He-Ne laser, coupled into the waveguide with a rutile prism. The TE-polarized beam is propagating in the X direction in the crystal.
Fig. 3. Photographs of OMA output, at input aperture 3 mm, showing intensity distribution in focal plane for lens of Fig. 1. Photos (a) and (b) show condensed and expanded horizontal scales, respectively, of the unexposed lens, while photos (c) and (d) show the condensed and expanded scales for the lens after exposure to 33 J/cm^2 uv radiation.

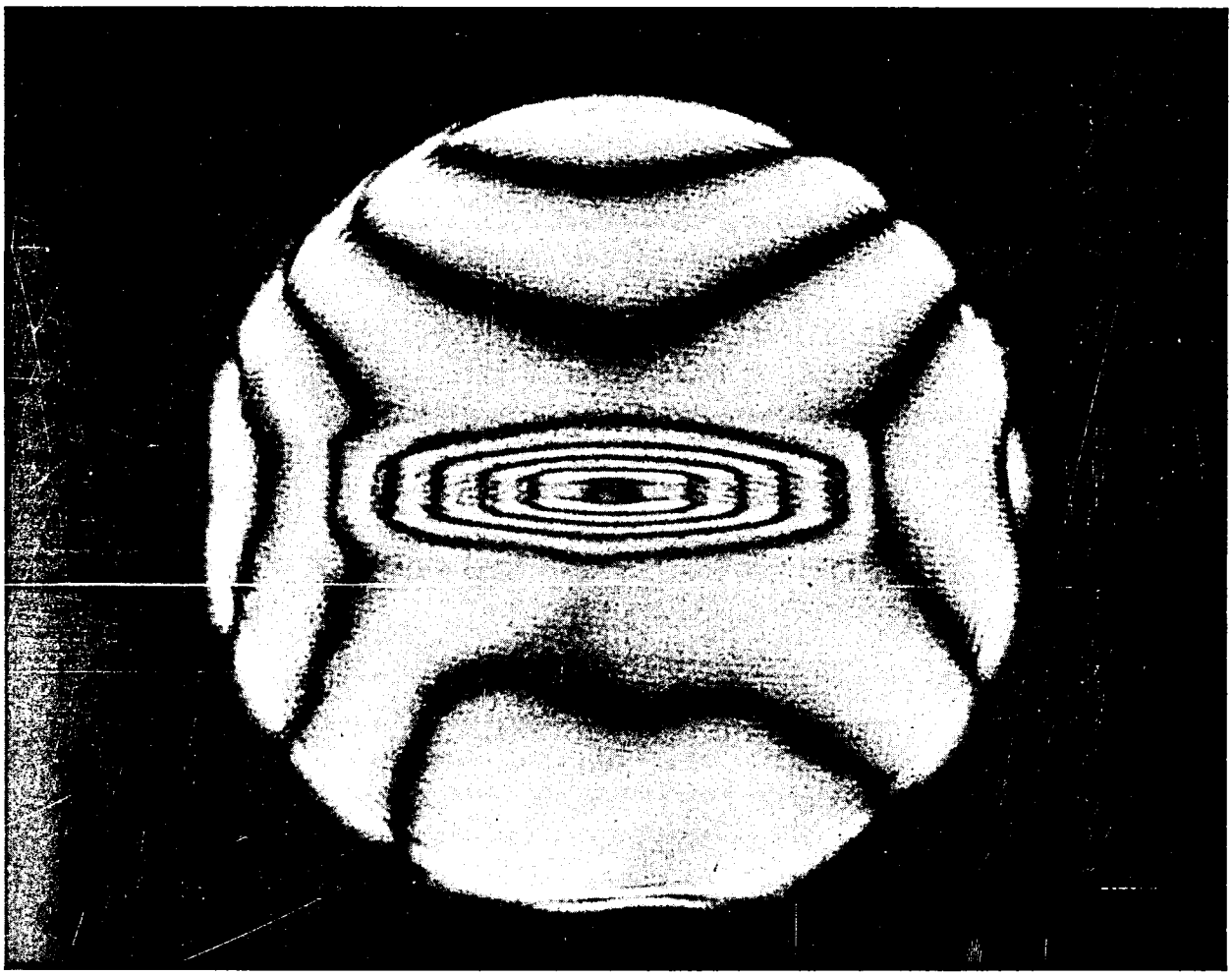

FIGURE 1.

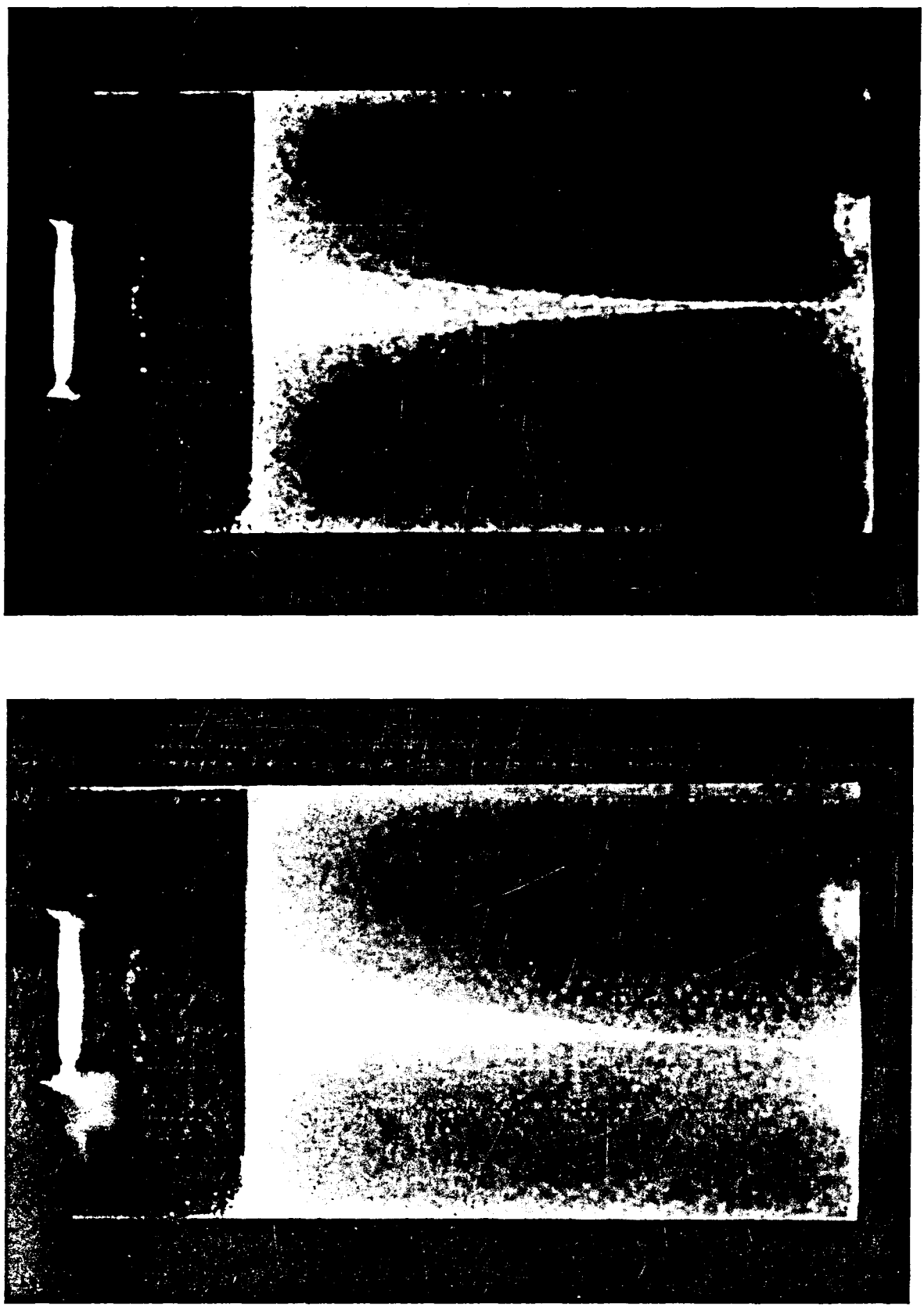

FIGURE 2.

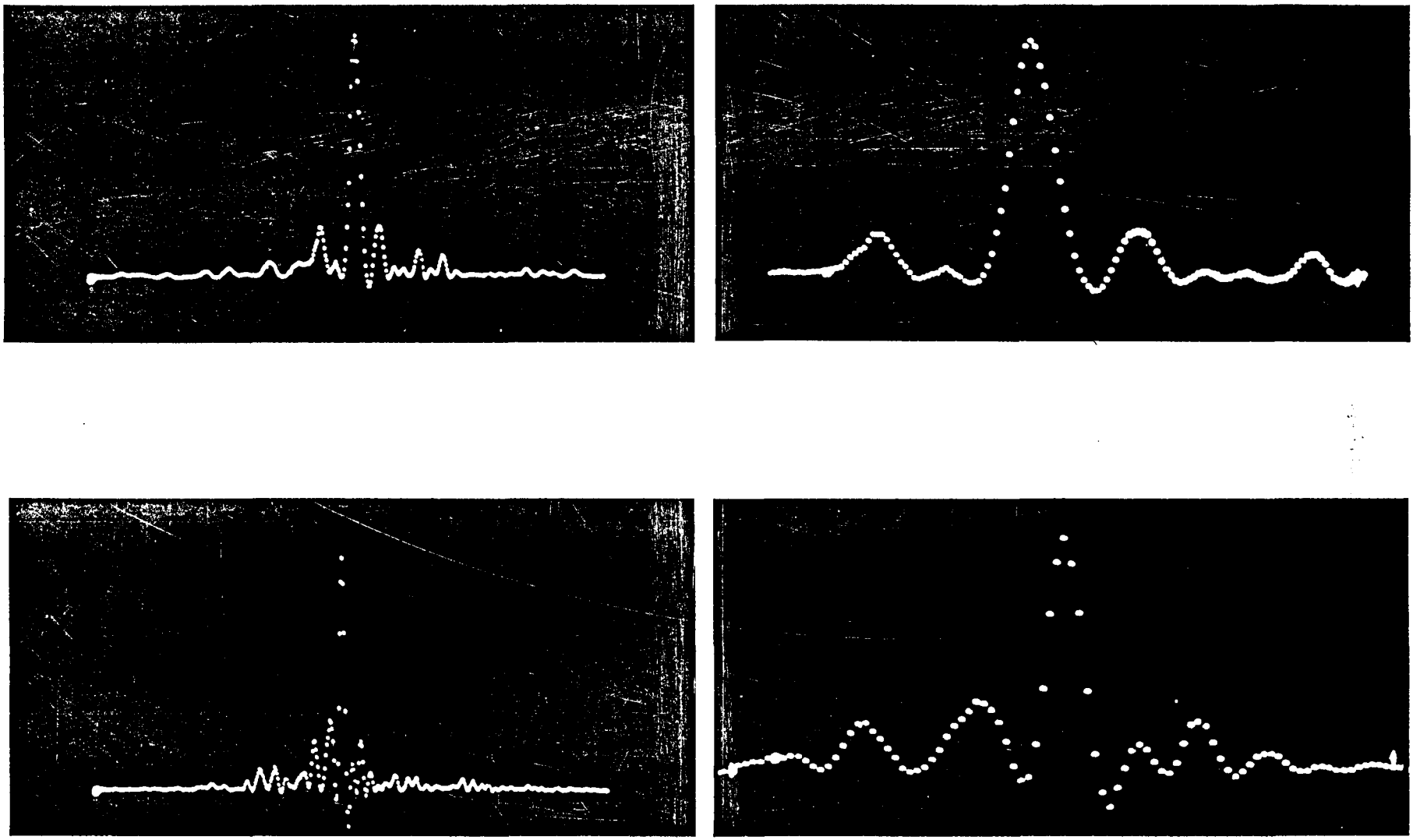

FIGURE 3.

APPENDIX C

PUBLICATIONS

APPENDIX C

PUBLICATIONS

1. James R. Busch, Van E. Wood, Richard P. Kenan, and Carl M. Verber, "Evaporated As_2S_3 Luneburg Lenses for $LiNbO_3$:Ti Optical Waveguides," Optical Information Processing for Aerospace Applications, NASA Conference Publication 2207 (NASA Scientific and Technical Information Branch, 1981), p. 251.

2. Carl M. Verber, James R. Busch, and Van E. Wood, "As_2S_3 Luneburg Lenses on $LiNbO_3$ Waveguides," J. Opt. Soc. Amer. 71, 1559 (1981) (abstract).

3. James R. Busch, Van E. Wood, Duncan T. Moore, Ben Woolley, and W. H. Southwell, "Rectangular Luneburg-type Lenses for Integrated Optics," Paper in preparation for submission to Optics Letters.

1. Report No.	2. Government Accession No.	3. Recipient's Catalog No.
NASA-CR-165972		

4. Title and Subtitle	5. Report Date
Design, fabrication, and evaluation of chalcogenide glass Luneburg lenses for $LiNbO_3$ integrated optical devices	September 1982
	6. Performing Organization Code
7. Author(s)	8. Performing Organization Report No.
Van E. Wood, James R. Busch, and Carl M. Verber	
	10. Work Unit No.
9. Performing Organization Name and Address	11. Contract or Grant No.
Battelle Columbus Laboratories 505 King Avenue Columbus, Ohio 43201	NAS1-16652
	13. Type of Report and Period Covered
12. Sponsoring Agency Name and Address	Contractor report, June 1981 - September 1982
National Aeronautics and Space Administration Langley Research Center Hampton, Virginia 23665	14. Sponsoring Agency Code

15. Supplementary Notes

Final Report

16. Abstract

Optical-waveguide Luneburg lenses of arsenic trisulfide glass have been made and tested. The lenses are formed by thermal evaporation of As_2S_3 through suitably placed masks onto the surface of $LiNbO_3$:Ti indiffused waveguides. The lenses are designed for input apertures up to 1 cm and for speeds of f/5 or better. They are designed to focus the TM_0 guided mode of a beam of wavelength, external to the guide, of 633 nm. The refractive index of the As_2S_3 films and the changes induced in the refractive index by exposure to short-wavelength light have been measured. Some correlation between film thickness and optical properties was noted. The short-wavelength photosensitivity has been used to shorten the lens focal length from the as-deposited value. Lenses of rectangular shape, as viewed from above the guide, as well as conventional circular Luneburg lenses, have been made. Measurements made on the lenses include thickness profile, general optical quality, focal length, quality of focal spot, and effect of ultraviolet irradiation on optical properties. The best lenses had speeds of f/3 to f/2, and possessed good to very good focal properties--central spots within twice the diffraction - limited intensity--when stopped down to f/10 to f/5. Preliminary investigations of information - handling capacity of some lenses were also carried out.

17. Key Words (Suggested by Author(s))	18. Distribution Statement
lithium niobate arsenic trisulfide glass integrated optics Luneburg lenses	Unclassified - Unlimited

19. Security Classif. (of this report)	20. Security Classif. (of this page)	21. No. of Pages	22. Price
Unclassified	Unclassified	51	

End of Document

NASA CR-165,974

NASA Contractor Report 165974

NASA-CR-165974
19830004124

COMPUTATIONAL MODELING OF MULTISPECTRAL REMOTE SENSING SYSTEMS: BACKGROUND INVESTIGATIONS

R. Martin Aherron

INFORMATION & CONTROL SYSTEMS, INCORPORATED
28 Research Drive
Hampton, Virginia 23666

Contract NAS1-16367
August 1982

National Aeronautics and
Space Administration

Langley Research Center
Hampton, Virginia 23665

TABLE OF CONTENTS

Page Missing in Original Document

LIST OF TABLES

Page Missing in Original Document

LIST OF FIGURES

1. INTRODUCTION

The following report represents background research for, and technical embellishments of, a comprehensive computational model of a multispectral remote sensing system. This model is being developed as a tool for designing smart sensors which are able to process, edit and classify the data that they acquired. This report provides a forum for details and analyses that have not been suitable for reporting in other formats during the progress of the work. Consequently the reader will be assumed to be familiar with both the computational model and experimental results reported up to this date; (Huck, et al., 1982 and Aherron, et al., 1981). In addition to the two above reports the AIAA (Breckenridge, 1979) and the SPIE (Barbe, 1979) have both published a collection of papers concerning smart sensors and the philosophy behind them.

Accurately predicting the signal produced by a sensor observing a particular target under a specific set of conditions is a very important goal for a model of this nature. Still more important is formulating a model that properly characterizes the stochastic properties of the signal that will likely be encountered. It is the physical nature of the interacting media that is considered to be variable and thus driving the derived quantities such as radiances. A quantity such as path radiance is not considered to have any inherent variability. Accounting for these variabilities introduced a special set of evaluation criteria in choosing a method of dealing with two of the major elements in the remote sensing system model: 1) atmospheric radiative transfer; 2) surface reflectance.

In particular the implementation of the simulation required that the sensor irradiance be calculated for every simulated pixel with its associated random atmospheric conditions, or equivalently the equation of transfer needed to be solved for every pixel simulated. This need of course discriminated heavily against lengthy iterative solutions to the transfer equation, accuracy not withstanding. An analysis of various atmospheric radiative transfer models will be presented.

It is impossible to over emphasize the importance of the spectral reflectance of the targets in remote sensing work. Nevertheless, given the

amount of research about and gathering of spectral reflectances taking place, particularly with respect to vegetation, it is amazing to find there is virtually no data report concerning the variability of spectral reflectances. Theoretical work concerning spectral reflectance has also been rather sparse. Several functional forms for reflectance variability will be examined and a collection of target reflectances will be cataloged.

A goal established early in the development of smart sensor systems was the ability to detect cloud pixels. This ability would allow several options concerning data load reduction or choosing alternate imaging sites. The category of snow/clouds can usually be distinguished in either the visible or near-infrared. To distinguish between snow and clouds alone requires a spectral channel at a wavelength longer than 1.0 μm.

The papers by Huck, et al., (1982) and Aherron, et al., (1981) cover two sets of experiments performed over the period of this contract. The Huck, et al. paper concentrated on classifying pixels into fairly specific classes such as wheat and dark loam. The Aherron, et al. paper concentrated on the task of assigning pixels from any number of different substances into four broad categories which were: bareland, water, vegetation and snow/cloud. An enhancement implementing aerosol attenuation coefficients has produced results updated from those in Aherron, et al. A partial set of updated results for that work are presented. Results for a simple cloud detection algorithm will also be presented.

2. COMPUTATIONAL ATMOSPHERIC RADIATIVE TRANSFER

2.1 Background

The atmosphere is a significant element in the overall remote sensing model. A comprehensive treatment of this element incurs the greatest computational costs of any model element. Numerous assumptions and simplifications are usually made to facilitate "reasonable" limits to the complexity and cost of radiative transfer modeling. Different sets of these assumptions are manifest in the various atmospheric models currently available. Below, a brief discussion is presented of the problem and several computational models in use in remote sensing are highlighted and compared. From these discussions the justification for the chosen model should be apparent. Those not familiar with the equations and terminology of atmospheric radiative transfer should consult Liou (1980) or Wolfe and Zissis (1978) for a background development. The terminology and notation used in this and related papers is almost identical to that used in Chapter 4 of Wolfe and Zissis (1978) which makes it particularly good as an introduction.

The fundamental equation of remote sensing after Slater (1980)

$$L = \frac{1}{\pi} E_o \, T_o \, \mu_o \, \rho \, T + L_d \, \rho \, T + L_p \qquad (2\text{-}1)$$

where $E_o \equiv E_o(\lambda)$ is the solar spectral irradiance at the top of the atmosphere, $T_o \equiv T_o(\lambda,\tau,\mu_o)$ is the atmospheric transmittance along the incident path from the sun to the surface (solar zenith angle = θ_o, $\mu_o = \cos\theta_o$); $L_d \equiv L_d(E_o,\lambda,\tau,\mu_o,\rho)$ is the diffuse sky spectral radiance which results from all radiation scattered downward onto the surface (i.e., integrated at the target over elevation and azimuth); $\rho \equiv \rho(\lambda)$ is the spectral reflectance of the surface (sometimes called "signature"); $T \equiv T(\lambda,\tau,\mu)$ is the atmosphere transmittance along the exitant path from the surface to the sensor (zenith angle = θ, $\mu = \cos\theta$); and $L_p \equiv L_p(E_o,\lambda,\tau,\mu_o,\mu,\phi)$ is the path spectral radiance which results from all radiation scattered upward along the path from the surface to the sensor. The other parameters are wavelength, λ, optical thickness of the atmosphere $\tau \equiv \tau(\lambda)$, and azimuth angle ϕ between the planes of incidence and exitance. The component of the total radiance L which arises

from radiation reflected from the target is referred to as the beam spectral radiance L_b, that is $L_b = L - L_p$, and $L_b \equiv L_b(E_o,\lambda,\tau,\mu_o,\mu,\rho)$.

Now the equation of radiative transfer for a plane parallel atmosphere (Malila, et al., 1971) is given by

$$\mu\frac{dL}{d\tau} = L(\tau,\mu,\phi) - \frac{\omega_o(\tau)}{4\pi}\int_0^{2\pi}\int_{-1}^{1} p(\tau,\mu,\phi,\mu',\phi')L(\tau,\mu',\phi')d\mu'd\phi' - (1-\omega_o(\tau))B(\tau) \tag{2-2}$$

where $\omega_o(\tau)$ is the single scattering albedo which is the ratio of the sum of the scattering coefficients to the sum of the scattering and absorption coefficients. $B(\tau)$ is the Plank radiation function for thermal self-emission. The single-scattering phase function $p(\cdot)$ can be described as a probability density function for the particular direction a photon will scatter relative to the original direction of travel. The function usually has a highly irregular (radially asymmetric) shape. The straight numerical solution of this equation is very time consuming. The first assumption made for even the complex form shown is that the atmosphere is plane-parallel, that is it is an infinite slab bounded below by the ground. For near-nadir looking sensor systems this is not an unreasonable assumption. Several uses of atmospheric radiative transfer models in the remote sensing literature and the methods of a solution for equation will now be examined. First, attention will be focused on the solution of the equation of radiative transfer as implemented in the various methods. Assumptions and approximations concerning the atmosphere will be discussed later.

2.2 Radiative Transfer Models

The models discussed will be limited to those that have received attention in the remote sensing literature. Probably the most widely known model is the one developed by Turner (Malila, et al., 1971 and Turner, 1974) used in early systematic remote sensing studies. Another model receiving more recent attention was developed by Dave (1978) and has been applied to both remote sensing problems, Dave (1979), and solar insolation. O'Neill, et al. (1977, 1978) implemented Liou's (1973) model and compared it to Turner's model and to actual LANDSAT data. Kiang (1980) implemented Hansen's (1969) model for tests concerning atmospheric effects on Thematic Mapper data. The other less general models were encountered, due to Otterman, et al. (1980), and

Lampley and Blattner (1978), upon which discussion will be delayed. Attention will be concentrated on those models that account for all the terms in Eq. 2-1. In dealing with the atmosphere in strictly a transmissive mode, that is accounting for only the first term in Eq. 2-1, LOWTRAN (Selby, et al., 1978) has become the accepted standard model.

The fundamental character of, and difference between most approximate methods of solution for the full equation is in the form and order of approximation of the phase function. This approximation is to allow the elimination of the integration in Eq. 2-2. The phase function determines the directional characteristics of all scattered radiation. Wolfe and Zissis (1978) show plots of some typical phase functions that demonstrate their pronounced asymmetry. Turner used two Dirac delta-functions one forward and one backward to approximate the phase function. Liou (1973) expanded the phase function into a series of N Legendre polynomials in his Discrete Ordinate Method (DOM). References to this model frequently are of the form "2N-stream approximation" where N is an integer. Dave (Dave and Canosa, 1974) used the method of Spherical Harmonics where the phase function and the intensity were expanded into a series of L + 1 Legendre polynomials. Krook (1955) shows that the DOM and Spherical Harmonic methods are equivalent. The accuracy of these equivalent methods can be made arbitrarily high by increasing the number of terms in the expansion (O'Neill, et al., 1977). The typical scattering phase function is a highly "peaked" function and thus rich in harmonics. In essence the Legendre based methods approximated the phase function with some finite set of polynomials (i.e., harmonics) while the Turner method approximated the function with an infinite set of harmonics in the form of the dirac-delta function. All of the above methods can be defined for a single homogeneous layer of any reasonable optical thickness. Hansen (1969) approximated the phase function at 20 discrete directions. The other fundemental difference is the intermediate solutions reached are valid only for an optically thin layer where multiple scattering can be ignored. The properties of an optically thick layer are arrived by aggregating the thin layers. Hansen's model accounts for polarization which is unique for the models discussed.

2.3 Model Comparisons

Ronnholm, et al. (1980) implemented a form closely related to each of the models discussed. The implementation of the radiative transfer models by Ronnholm, et al. assumed several things about the atmosphere. First an analytical form for the "real" phase function was used (Henyey-Greenstein). Second, the atmosphere was assumed to be vertically and horizontally homogeneous. All of the models except Turner's have been implemented with vertical inhomogeneity capabilities but this restriction was necessary for comparison. Each model was run for the same set of atmospheric conditions. (The Ronnholm, et al. literature citations will not be duplicated). Ronnholm, et al. used Twomey's doubling method model as a benchmark or "truth" so to speak, considering it to be more accurate than the other methods compared. Hansen's (1969) and Twomey's models are comparable. A delta-Eddington approximation by Joseph was included which is similar to the Turner model. The Discrete Ordinate Method for 4 streams was implemented using the analytical solution (Liou, 1974). Since the form of the differential equations solved for the DOM and Spherical Harmonics methods are similiar, the DOM's computational times will be considered representative of the Spherical Harmonics Method (when L = N).

One of the major findings of Ronnholm, et al. was the relative computational burden for the three classes of methods. The results are summarized in Table 2.1. The results in Table 2.1 can only be meaningful within the context of the relative accuracy of the various methods. Ronnholm, et al. compare the three methods for various conditions and concludes "... the factor of 20 in computation time saved by the delta-Eddington was judged more valuable than the greater accuracy of the four-stream method." They add "... if optical depths, single scattering albedos or asymmetry factors are either uncertain or known to be flucuating; with relative standard deviations of 10% or greater, then little real benefit is added by the use of computationally precise, but costly, many-stream radiation-transfer algorithms." An important point that should be made here, is that Ronnholm, et al. compare values of reflection, diffuse transmission, and absorption for the atmosphere and thus net fluxes are being compared. For aerosol laden atmospheres, and their highly anisotropic scattering properties, the jump from

TABLE 2.1

Relative computation burden of radiative transfer models used by remote sensing investigators analogy to methods implemented by Ronnholm, et al.

INVESTIGATOR	RONNHOLM'S ANALOG	REL. COMPUTER TIME
TURNER	DELTA-EDDINGTON	1
LIOU	DOM	20
DAVE	DOM	20
KIANG	TWOMEY	10^4

comparing fluxes to comparing intensities with directional dependences is not straight forward. For example, the radiation field incident on a scattering volume has only two components in a two stream approximation and for highly anistropic scattering this is an inadequate approximation for calculating the scattering into the highly specific direction of the sensor. In general, the more anisotropic the scattering phase function, the more accurately it needs to be approximated in order to determine the radiation field within the atmosphere. For the Turner model, the radiation field within the atmosphere is approximated utilizing the double-delta phase function. The actual path radiance contribution of a scattering volume is calculated using that simplified radiation field and interpolated values of the scattering phase function. The hemispherical integration for flux quantities implicit in Ronnholm, et al. tends to mask the inaccuracies. This provides some explanation for the disagreement between Ronnholm, et al., who found little difference between methods for flux quantities, and O'Neill, et al., who found significant differences between the predicted path radiances for the DOM and Turner's model. Even so the remarks by Ronnholm, et al. concerning the uncertainty about atmospheric conditions should not go unheeded, particularly for the case of errors in approximations of the scattering phase function.

It is useful to elaborate on the efforts of O'Neill, et al. concerning calculation of path radiance (O'Neill, et al. 1977, 1978). In O'Neill, et al. (1977) Turner's method and Liou's DOM were implemented assuming vertical homogeneity. The results were fairly comparable for low aerosol optical depths but were divergent as optical depth increased. They attributed this to the crude angular approximations used by Turner and their increasing importance at greater optical depths. In O'Neill, et al. (1978) path radiances computed by the DOM were found to be in good agreement with path radiances determined from LANDSAT data using clear lake reflectors. The DOM performed considerably better than the Turner method for the same set of data. Horvath, et al. (1972) found that the Turner method had systematic errors in predicting atmospheric effects on aircraft multispectral scanner data. The input data used in Horvath, et al. was not of as high a quality as for the O'Neill, et al. work.

The assumption of vertical homogeneity within the atmosphere does not seem plausible considering the distribution of aerosols. Neither Ronnholm, et al. (1980) nor Liou (1975) could demonstrate much difference in modeling results, for flux related quantities, between the lesser and more "accurate" methods of calculation. No test of the assumption's effect, in terms of model results, on radiance values was found. O'Neill, et al. achieved good agreement between LANDSAT determined and model predicted path radiances under the vertical homogeneity assumption.

By far the more important atmospheric constituent in terms of its effect on remote sensing is the aerosols. In certain wavelength regions though, absorption by other constituents becomes important. The major ones being water vapor, ozone, and oxygen in the visible and near infrared regions. Accurately accounting for absorption by the constituents is not a trivial task (Selby, et al., 1978; Dave, 1978). Turner treats the ozone absorption, occuring in the upper atmosphere, as a phenomena separate from the scattering, which takes place in the lower atmosphere. Except for Turner those models that do deal with molecular absorption utilize the Air Force Geophysics Lab's model LOWTRAN (Selby, et al., 1978) or data from that model.

2.4 Special Models

As was mentioned before, two other less general models of transfer were found in the literature. The Otterman, et al. (1980) work was mostly illustrative in nature, dealing only with low optical thickness atmospheres, and is rather unique in its solution. Both Otterman, et al. and Lampley and Blattner (1978) deal only with single scattering. This assumption greatly simplifies the characterization of the radiation field within the atmosphere. For the case of optically thin atmospheres this is not a bad assumption but likely to be encountered only in more arid regions on a regular basis. This assumption, for thin layers, is the basis of the doubling method discussed earlier. Eliminating the effects of multiple scattering is judged to be too large a source of error when dealing with atmospheres optically thick enough to cause significant image degredation.

2.5 Model Selection

One of the evaluation criteria set for evaluation of various atmospheric models was their suitability for use as a computer subroutine for a remote

sensing system simulation. One other approach suggested by O'Neill, et al. (1978) and inferred by Dave (1978) is the use of table-lookup method. For certain problems this could be a very useful technique. But for a general purpose source of radiance data for a stochastic simulation, with many of the input parameters being random variables, it would likely prove excessive in its storage requirements. To define the size of radiance data base needed to satisfy the modeling requirements would require knowledge as to how fine a grid, or subdivision, in each parameter, would be necessary to retain the desired accuracy. This knowledge is not available a priori and would only come from careful and laborious sensitivity analysis for the input parameters. It may be possible to gain increased accuracy, over say the Turner model, by implementing a table lookup scheme for a more accurate model but it would be better to pay the greater price for the subroutine method and get the full benefit of increased accuracy.

From what has been discussed one can see that the Turner model of radiative transfer introduces significant errors to the approximation of sensor incident radiation compared to other more comprehensive models (i.e. DOM). There is though, an estimated twenty fold reduction in computing time realized. Whether or not the error introduced by the Turner model is significant in the light of the uncertainties in the atmospheric parameters has yet to be determined. Ronnholm, et al. showed that, for flux calculations, these errors were not significant. For an initial implementation of a model with multiple scattering capabilities within a comprehensive remote sensing system model, the Turner model is the logical choice. Once greater knowledge of the interrelationships and sensitivities of the various system entities is established, it would probably be best to upgrade to the Dave model.

2.6 Model Implementation

The Turner model was implemented as a subroutine within the computer simulation code. The model is available for purchase from the Environmental Research Institute of Michigan (ERIM) located in Ann Arbor, Michigan. Scattering phase function data files which are distributed with the model were used. Input to the Turner model, as implemented, consists of nine parameters and one function (table form). Those parameters considered to be deterministic

(fixed for a particular run) were E_o - Solar Irradiance, θ_o = Solar Zenith Angle, ϕ = Azimuth angle between incident and exitant vectors, θ = Sensor Zenith Angle, ω_o = Single Scattering Albedo. The scattering phase function was also deterministic. All simulation to date have been performed with phase functions from a continental type aerosol model with a complex index of refraction of m = 1.5 - .01i. The single-scattering albedo was chosen to be .9 and is constant. Simulations have been confined to nadir looking sensors with solar zenith angles in the range of 30° - 50°.

There are four stochastic parameters consisting of ρ_b = background reflectance, ρ_T = target reflectance, τ_R = Rayleigh optical thickness and τ_T = total optical thickness. The background used was a bare land target. Both reflectances are generated according to the functional form discussed earlier. The optical thicknesses are generated by the method discussed in Huck, et al. (1982). It is necessary to separate the Rayleigh component because the phase function used is a weighted mean of the Rayleigh and aerosol phase functions.

The single-scattering albedo used is constant over wavelength which requires a word of warning. The single-scattering albedo defines the relative mix of scattering and absorption in the contribution to attenuation. Therefore in moving from spectral regions characterized by scattering to those with significant absorption the single-scattering albedo changes. A method for varying the single-scattering albedo has not been implemented. The single-scattering albedo chosen (.9) is reasonable for regions of the spectrum without significant absorption. It is therefore necessary to restrict radiative transfer modeling to non-absorbing regions at the present time.

3. SPECTRAL REFLECTANCE MODELS

Ultimately it is the spectral reflectance characteristics of targets, perhaps in concert with spatial distribution characteristics, that provides the information to users of remotely sensed data. It is therefore important that the target reflectance properties introduced to a simulation be as realistic as possible. This is particularly true for optimization studies where optimizing a system for a set of "artificial" targets is of more academic interest than practical use.

There were two major tasks to be addressed in the area of reflectances. One concerned characterizing the deterministic nature of spectral reflectances which consisted of assembling representative spectral reflectance curves for a number of targets of interest. The other task dealt with characterizing the stochastic nature of spectral reflectances by selecting and parameterizing functional forms for describing reflectance variability.

3.1 Reflectance Functions

The quantity utilized in the simulation is the spectral diffuse reflectance defined by Slater (1980).

$$\rho(\lambda) = \frac{\pi L (\lambda)}{E (\lambda)}$$

where the target is assumed to have Lambertian characteristics. The quantity actually measured in the field, depending on the particular measurement program, is more likely the hemispherical-conical reflectance factor which is then normalized to some standard reflector (Smith and Ranson, 1979). Present work has been limited to the Lambertian target assumption though natural targets have been demonstrated to deviate significantly from this assumption (Smith and Ranson, 1979). In general Slater (1980) offers a very good introduction to surface reflectance and its importance in remote sensing and presents a brief introduction to several efforts aimed at modeling plant canopy reflectance. Smith and Ranson (1979) offers a fairly comprehensive review of the literature concerning data and/or models of the directional reflectance characteristics of natural surfaces.

In order to produce spectral reflectances with stochastic characteristics

it was necessary to choose an analytical form for reflectance. The functional form chosen for the reflectance is given by

$$\rho(\lambda) = \rho_o(\lambda)\, e^{-\beta_o(\lambda)X} \tag{3-1}$$

This is the same functional form (Bouguer's Law) as used for atmospheric transmission. The wavelength dependence of reflectance will be omitted in subsequent notation. This form was used because of its analytical tractability and compatibility with the concurrent atmospheric modeling efforts and because the family of curves generated were qualitatively similar to sets of field data (Park, et al., 1980). The parameters of the distribution are $\rho_o(\lambda)$ and $\beta_o(\lambda)$. This is identical to a form for spectral reflectance proposed by Tucker and Maxwell (1976) for vegetation canopies in regions of the spectrum characterized by canopy absorption (i.e., the chlorophyll absorption regions). Within the same spectral region and dependent on the value of X, Tucker (1977) and Tucker and Maxwell (1976) found that

$$\rho = \rho_o + \beta_o X^{-1} \tag{3-2}$$

was also a useful functional relationship.

In Tucker's work X represented any one of several plant canopy characteristics including several biomass measures, leaf water content and chlorophyll content. For the near infrared region from .74 m to 100 m which is characterized by little absorption and relatively high reflectance due to scattering, Tucker (1977) found, again dependent on the value of X, the following two equations to be good approximations of reflectance

$$\rho = \rho_o + \beta_o X \tag{3-3}$$

$$\rho = S\,(1 - e^{\rho_o + \beta_o X}) \tag{3-4}$$

Where S represents the asymptotic reflectance of the vegetative canopy. This is the reflectance that an infinitely thick canopy would display. Park and Deering (1981) developed a set of differential equations (modifications of the Kubelka-Munk model) for describing the interaction of light with

plant canopies that is remeniscent of the Eddington Approximation for atmospheric radiative transfer. If the background reflectance is taken to be zero then the diffuse reflectance formula of Park (retaining previous notation)

$$\rho = \frac{1 - e^{-\beta_o X_o}}{\frac{1}{S} - Se^{-\beta_o X_o}} \qquad (3\text{-}5)$$

Of the above functional forms, only Eqs. 3-2, 3-3, and 3-4 display asymptotic nature. Equation 3-2 asymptotes for large values of X and Eqs. 3-3 and 3-4 asymptote for small and large positive values of X. Ideally if X is some vegetative measure such as biomass per unit area then the reflectance functions should asymptote to the background reflectance for small X and approach the vegetative reflectance asymptote for large X. These three equations were formulated to be driven by inherently positive plant characteristics such as canopy weight. Equation 3-1 is driven by an artificial variable taking positive and negative values. As was previously stated, the resulting curves were qualitatively acceptable.

Target reflectance phenomenon represent a special case of radiative transfer, a subject which has received a great deal of attention over the years. Commenting on the dearth of surface reflectance modeling efforts Smith and Ranson (1979) hypothesize "probably, this is a recognition of the difficulty of specifying the appropriate phase function in both a sufficient and tractable manner and further, performing the necessary measurements to determining the phase functions". They were commenting on the difficulty of specifying and measuring the phase function of such things as twigs and leaves. Smith and Ranson (1979) discuss the formulation development of two major vegetative canopy models, Smith and Oliver (1972) and Suits (1972), taking care to link the "... analytical and physical reasoning of canopy radiation interactions to the broader mainstream of radiative transfer theory". A better understanding and overview can be gained by reading their unified discussion prior to working with the original papers. The radiative transfer methods used in these models can be classed as those that use simplistic approximations to the phase function such as the Eddington approximation.

The following development outlines the parameterization of Eq. 3-1.

We assume X_o is a (standard) normal random variable with mean $\mu_\rho = 0$ and variance $\sigma_\rho = 1$. Repeating the formula for reflectance. The assumption of normality for X will be discussed more completely in a later section. When X is assumed to be a normal variate the reflectance, given by Eq. 3-1, has a log-normal distribution.

$$\rho = \rho_o e^{-\beta_o X} \tag{3-6}$$

then

$$\mu_{1\rho} = \rho_o e^{-\frac{1}{2}\beta_o^2} \tag{3-7}$$

$$\sigma_\rho = \mu_\rho^2 \left(e^{\beta_o^2} - 1\right) \tag{3-8}$$

If we have estimates for μ_ρ and σ_ρ denoted $\hat{\mu}_\rho$ and $\hat{\sigma}_\rho$, respectively, then by substituting the estimates into the above formulas yields estimates of the parameters.

$$\beta_o = \sqrt{LN\left(1 + \frac{\hat{\sigma}_\rho^2}{\hat{\mu}_\rho^2}\right)} \tag{3-9}$$

$$\rho_o = \frac{\hat{\mu}_\rho}{\sqrt{1 + \frac{\hat{\sigma}_\rho^2}{\hat{\mu}_\rho^2}}} \tag{3-10}$$

Finding data to define the variability of spectral reflectances (i.e., σ_ρ) has not been very fruitful. As of yet, no data has been found on the covariance (between wavelengths) of spectral reflectance for various targets. Values for the variance (i.e., the diagonal terms of the covariance matrix) can be estimated from data, for wheat, reported by Collins (1978) through the following reasoning as shown below.

A simple expression for the remote sensing equation for vertical sun and sensor can be defined as

$$L = \frac{1}{\pi} E_o T^2 \rho + Lp$$

(With notation as before in atmospheric section). Over small geographical areas it can be assumed that all the terms are constant except ρ. Allowing the calculation of

$$\sigma_L = \frac{1}{\pi} E_o T^2 \sigma_\rho$$

$$L = \frac{1}{\pi} E_o T^2 \bar{\rho} + \bar{L}p$$

Collins reports data for medium altitude aircraft in a fairly dry area (Imperial Valley) thus Lp is ignored and thus dividing Eq. 3-12 by Eq. 3-3 gives

$$\frac{\sigma_L}{\bar{L}} = \frac{\sigma_\rho}{\bar{\rho}} = \text{Coefficient of variation (CV)}$$

Collins reports CV as percent standard deviation of measure radiance which determines $\frac{\sigma_\rho}{\rho}$ necessary for formulas 9 and 10. Since Collins was working with radiances an estimate of $\bar{\rho}$ necessary for Eq. 3-10 is not available.

Rao, et al. (1978) similarly reported reflectance CV's for grain crops and soil. The data was for variation over several months and encompassed atmospheric corrections of unknown nature making it unsuitable for present efforts. A CV of .1 was chosen for all agricultrual crops after reviewing Collins data.

As a note of explanation, Smith and Oliver (1972) developed a stochastic vegetation canopy model but more appropriately should be termed a Monte Carlo model in that the photon interaction with various canopy constituents (canopy orientation and distribution) was treated as a random process but then the canopy composition was constant and thus is fundamentally different than the model being discussed.

So far discussions of reflectance have centered on vegetation. The same function was also used for the other targets. For soil Condit (1970) was a valuable source of spectral reflectances. The nature of the curves presented allowed an estimate of reflectance variability to be made. Each soil was characterized by two spectral reflectance curves: one for dry

soil and one for wet soil. The mean and variance for that soil was determined by the following

$$\hat{\mu}_\rho = \frac{\rho_{dry} + \rho_{wet}}{2}$$

$$\hat{\sigma}_\rho = \frac{\rho_{dry} - \rho_{wet}}{2}$$

In general, variances were chosen for other targets in order to achieve "Reasonable families" of curves in a stochastic simulation. One significant modification of the parameters was made for vegetation. The reflectance variability σ_ρ was made proportional to reflectance. That is CV was constant (.1) and multiplied by $\bar{\rho}$ to yield σ_ρ for estimating β_o and ρ_o. The effect of this modification can be seen in the difference in variability behaviour between vegetation and sand in Fig. 4 of Huck, et al. (1982). As one can see this introduces variations in σ_ρ over wavelength. It should be noted that the ± sigma plots of Fig. 4 (Huck, et al., 1982) are for $\pm\sigma_x$ and not $\pm\sigma_\rho$ such that they enclose ≃67% of the simulated reflectance values even though ρ is not normally distributed. This should become clear in the section on statistical characteristics.

The reflectance covariance matrix Σ_ρ for targets in general is defined as

$$\Sigma_\rho = \sigma_\rho^2 \, I_n$$

for

$$\lambda_i \qquad i = 1, 2, 3, \ldots, n$$

and where I_n = n x n identity matrix and σ_ρ is constant, but defining

$$\bar{\rho}^2 = \begin{bmatrix} \bar{\rho}^2_{\lambda_1} & & & & 0 \\ & \bar{\rho}^2_{\lambda_2} & & & \\ & & \bar{\rho}^2_{\lambda_3} & & \\ & & & \ddots & \\ 0 & & & & \bar{\rho}^2_{\lambda_n} \end{bmatrix}$$

and $CV = \frac{\sigma_\rho}{\bar{\rho}}$

the covariance matrix for vegetation is

$$\Sigma_\rho = CV^2 \, I_n \, \bar{\rho}^2$$

where CV is taken to be constant.

It is particularly important that the off-diagonal terms of the reflectance covariance matrix be approximated in future work and especially for investigation concerning the optimum choice of spectral channels. It has frequently been observed, or bemoaned if you will, that several of the LANDSAT channels are redundant. This is due in part to the high correlation of reflectance in the different channels. For example both LANDSAT channel 6 (.7 - .8) and channel 7 (.8 - .11) fall in the spectral region for vegetation characterized by the same reflectance phenomenon. Thus changes in the nature of the plant that affect reflectance in channel 6 affect channel 7 in almost the same way. This spectral reflectance correlation for channel 6 and channel 7 is true for most targets and therefore one of the channels is fairly redundant.

Wiersma and Landgrebe (1979) make an important contribution to remote sensing where they "develop an analytical procedure for the design of the spectral channels for multispectral remote sensor systems". Though never explicitly stated, it appears their analysis is based on spectral radiance data. The important point to this discussion is that they chose an optimal (mean-square) set of spectral channels where the analysis was based on the spectral radiance covariance matrix and is aimed at reducing channel redundancy. By reducing correlation between the channels they increase the information available from a fixed number of channels. This is shown by the techniques of Information Theory. Their radiance data does not allow the estimation of the spectral reflectance covariance necessary for the present modeling efforts.

3.1 Target Reflectance Curves

As was indicated, the target reflectances represent an important element in the remote sensing simulation. A collection of target reflectances

was gathered and subsequently used in simulations reported to date. Data collected was limited to in situ reflectances for single or collections of whole plants. Only data available in the open literature was utilized. There exists a large body of reflectance data produced for NASA, in raw form, that has yet to be utilized.

Examination of remote sensing literature from the early 60's to present shows the tendency to report reflectances to longer wavelengths in the infrared. Even with this tendency, very little reflectance data is published for wavelengths longer than 1.1 μm which happens to correspond to the limit of LANDSAT spectral coverage. Some data utilized in the cloud detection tests, which required data out to 1.60 μm, was of rather crude spectral resolution especially in the .50 μm to .80 μm range that is so important for the BAM categorization discussed in Aherron, et al. (1981). The sources of reflectance data are listed in Table 3.1 along with the figure number(s) for the plot(s) of that data.

TABLE 3.1

REFLECTANCE DATA

FIGURE NUMBERS	SOURCE OF DATA
FIG. 3.1 - 3.4	Lansing, 1970
FIG. 3.5 - 3.6	Condit, 1970
FIG. 3.7	Vlcek, 1974
FIG. 3.8	Suits and Safir, 1972
FIG. 3.9 (Silt Loam)	Bowers and Hanks, 1965
FIG. 3.9	Orr, et al., 1963
FIG. 3.10	O'Brien and Munis, 1975
FIG. 3.11	Hansen, 1969
FIG. 3.12	Novosel'tsev, 1965
FIG. 3.13	Leeman, et al., 1971

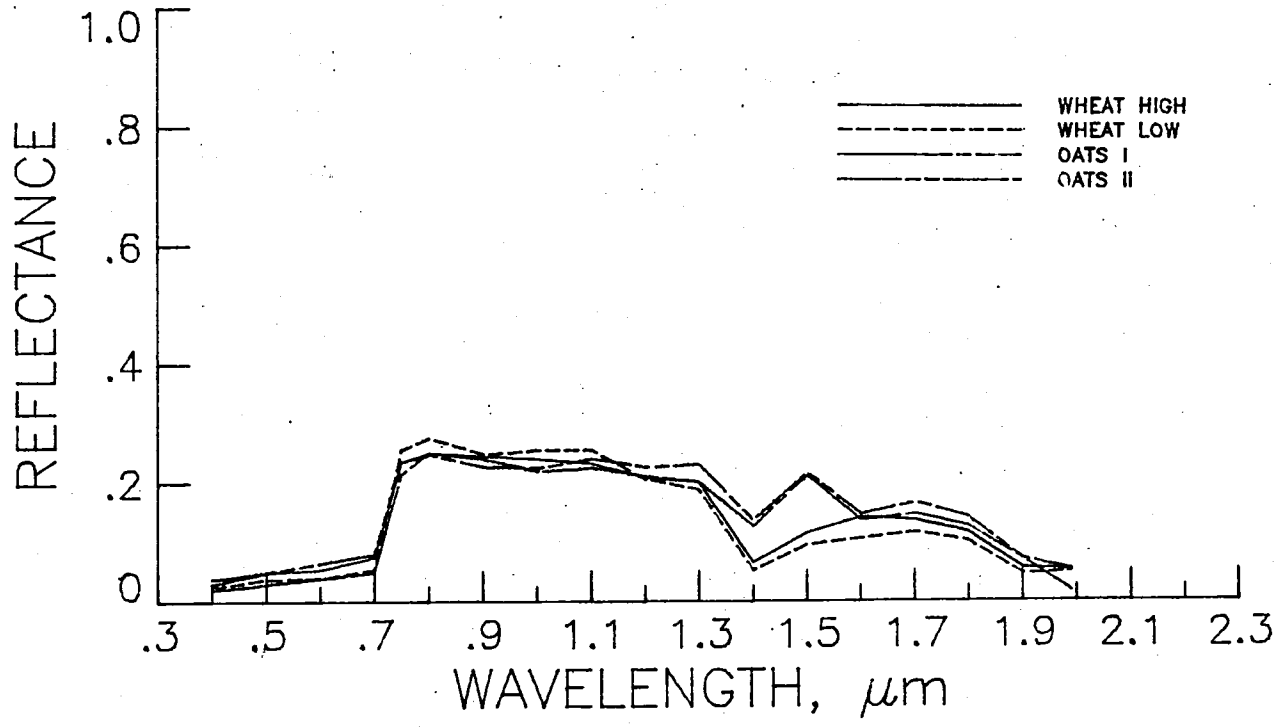

FIGURE 3.1 SPECTRAL REFLECTANCES

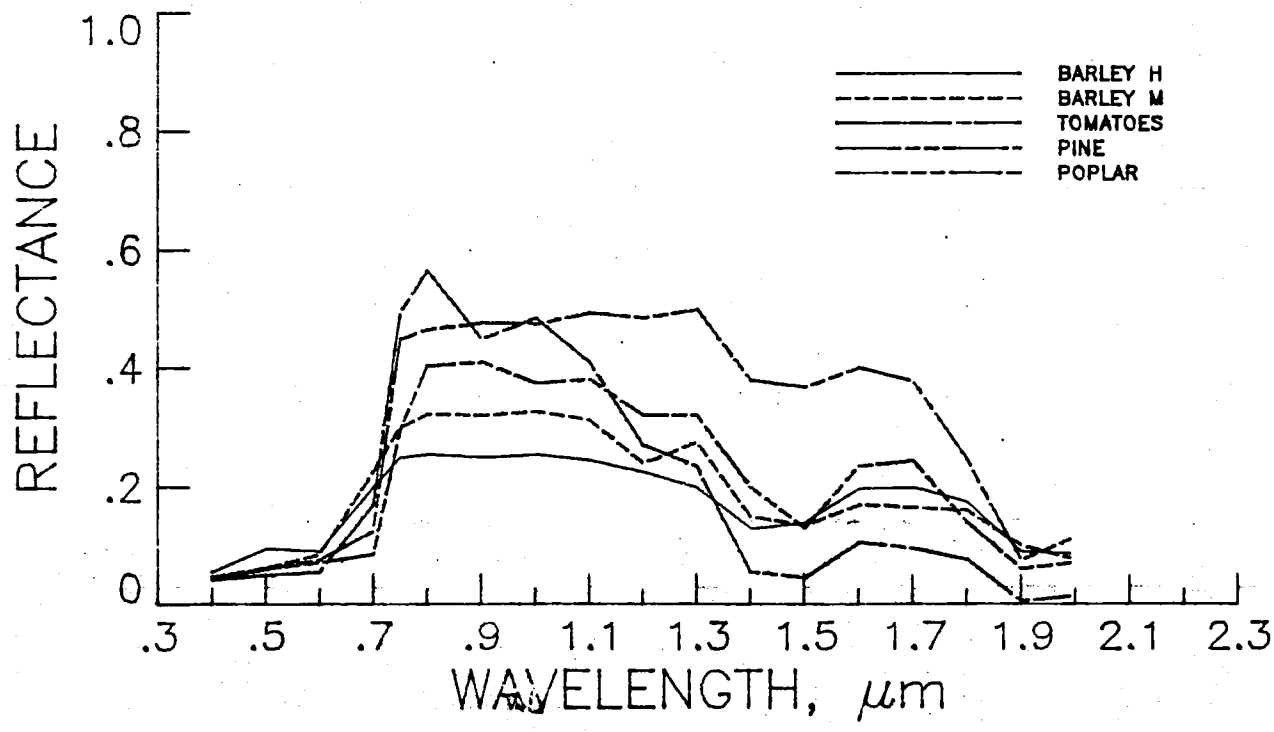

FIGURE 3.2 SPECTRAL REFLECTANCES

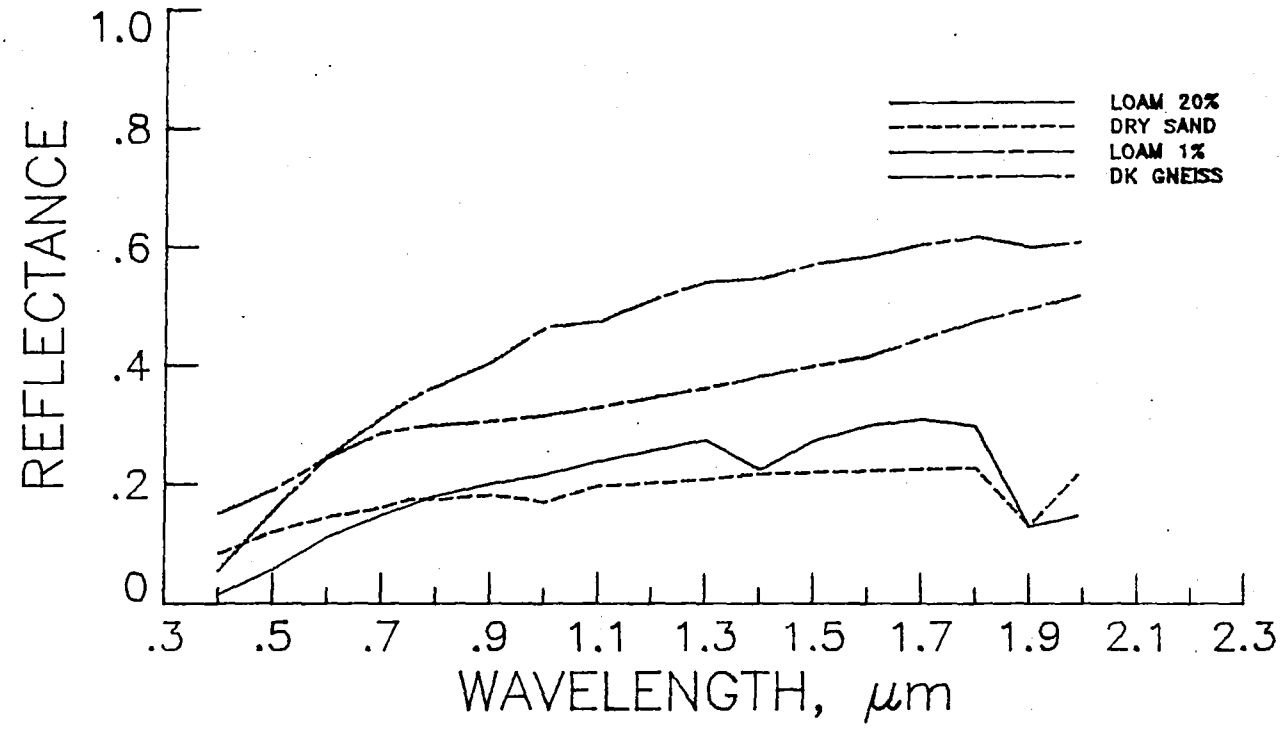

FIGURE 3.3 SPECTRAL REFLECTANCES

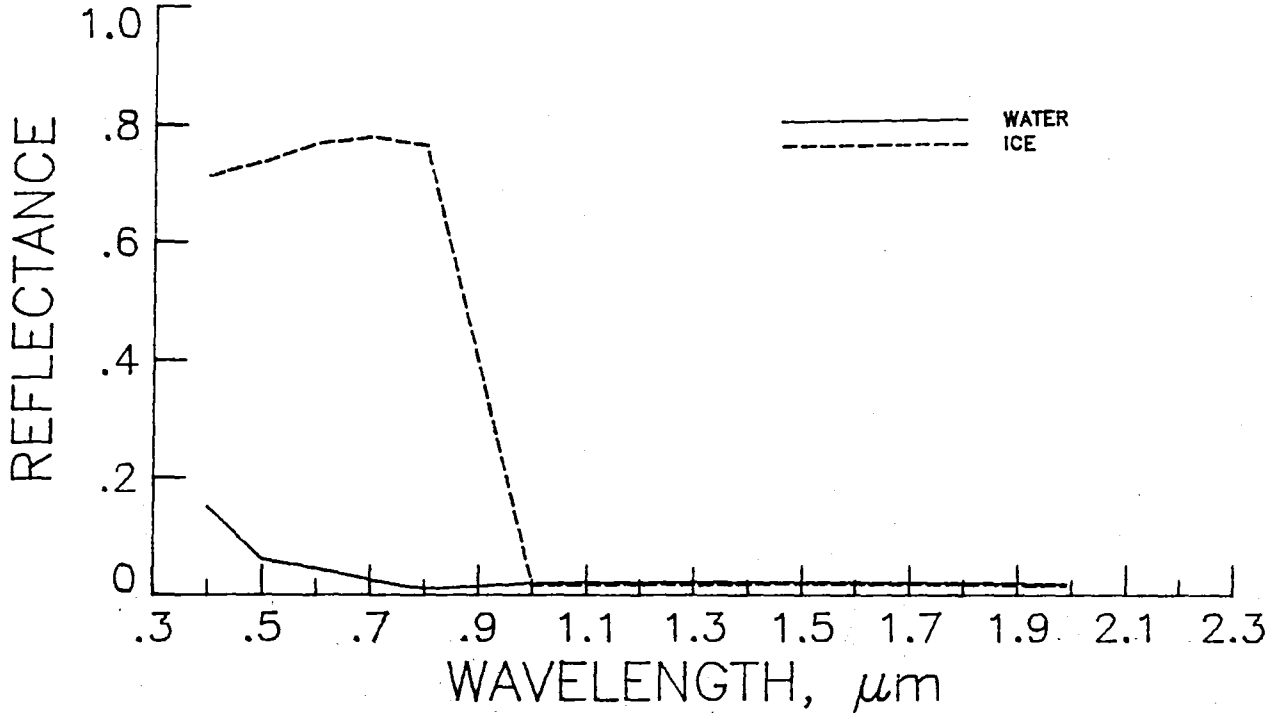

FIGURE 3.4 SPECTRAL REFLECTANCES

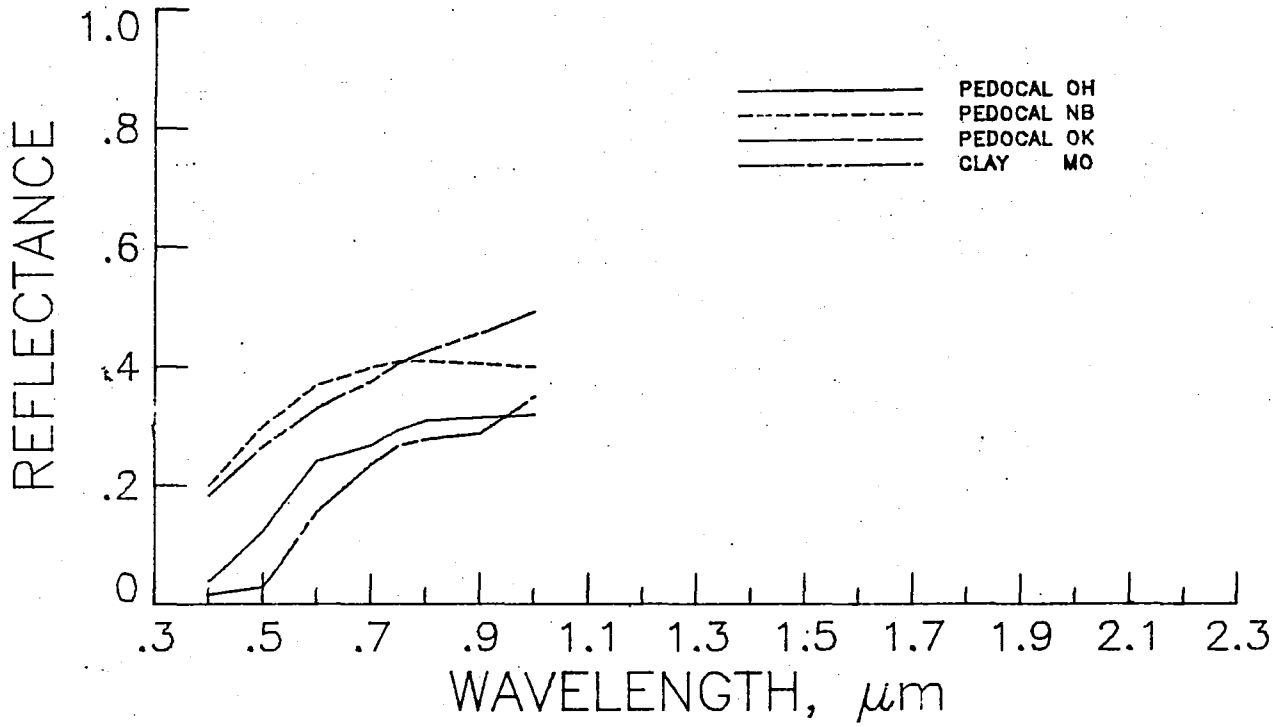

FIGURE 3.5 SPECTRAL REFLECTANCES

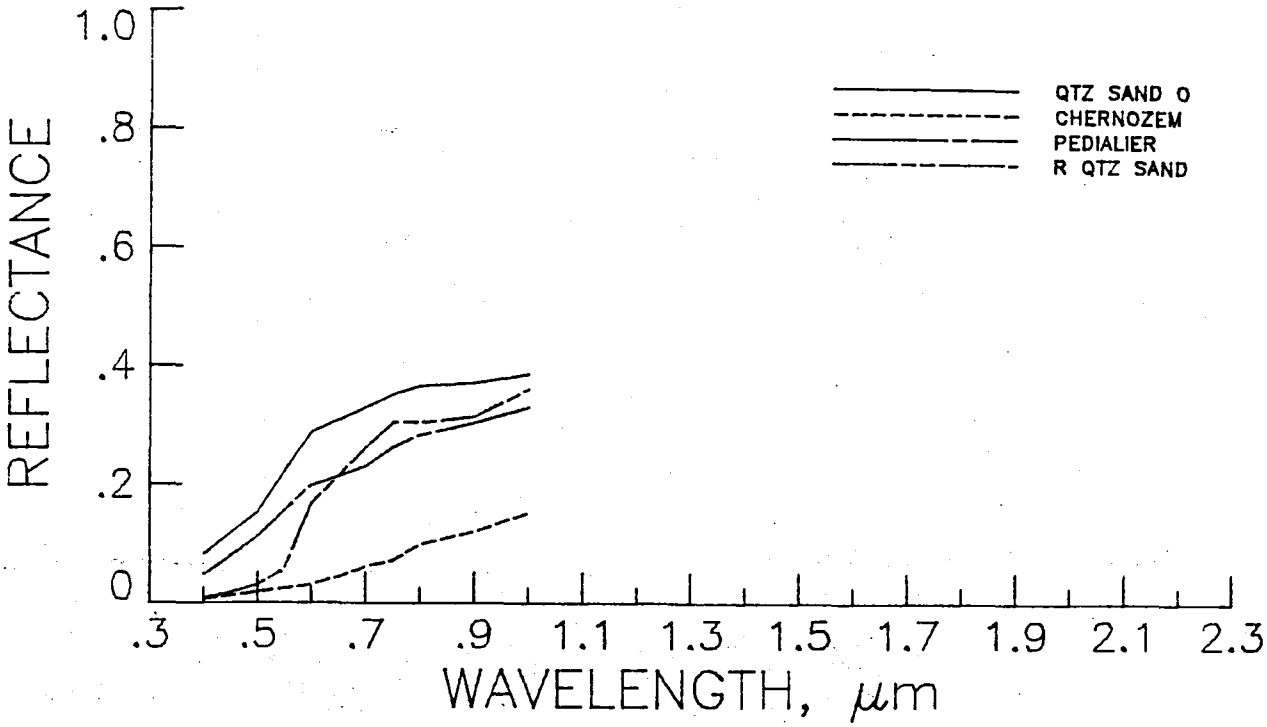

FIGURE 3.6 SPECTRAL REFLECTANCES

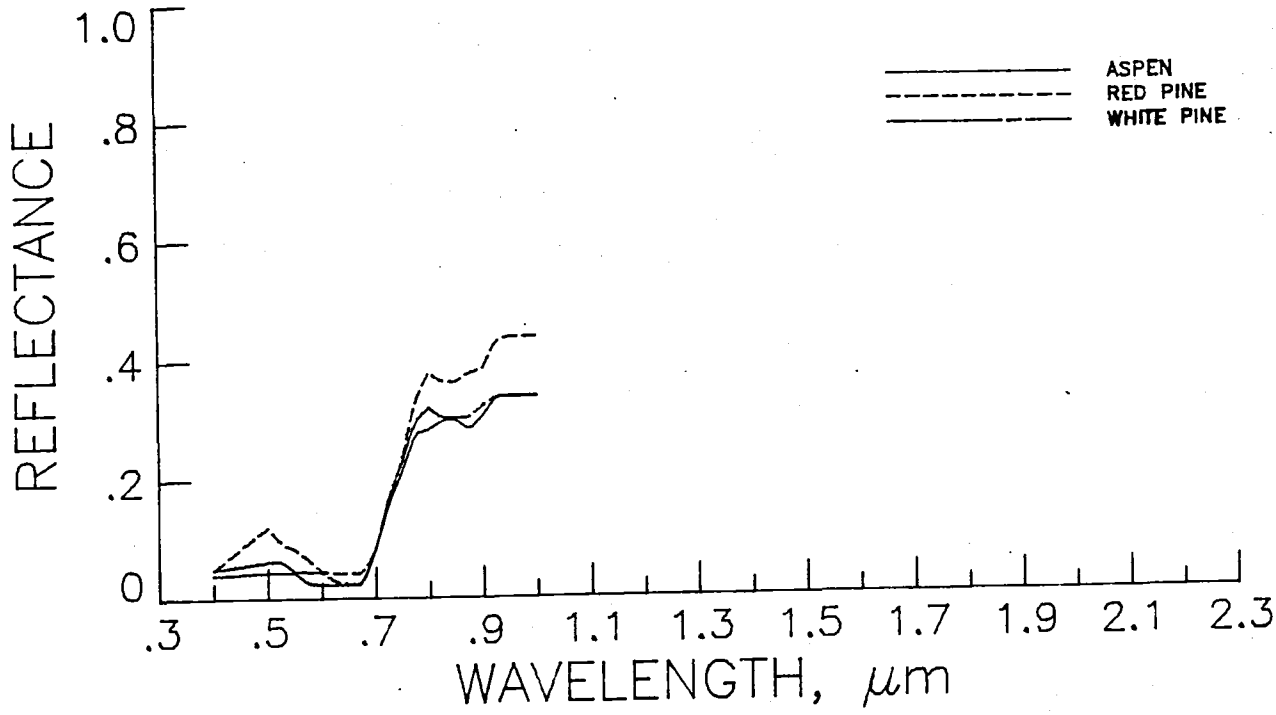

FIGURE 3.7 SPECTRAL REFLECTANCES

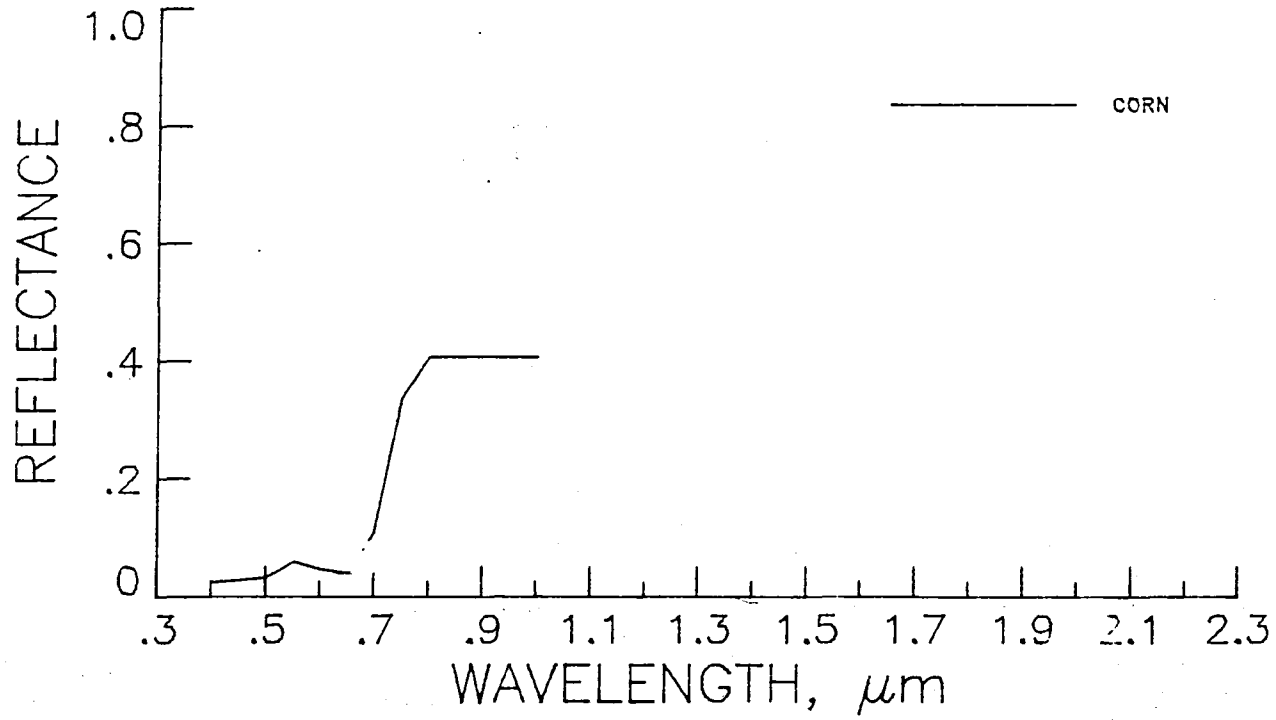

FIGURE 3.8 SPECTRAL REFLECTANCES

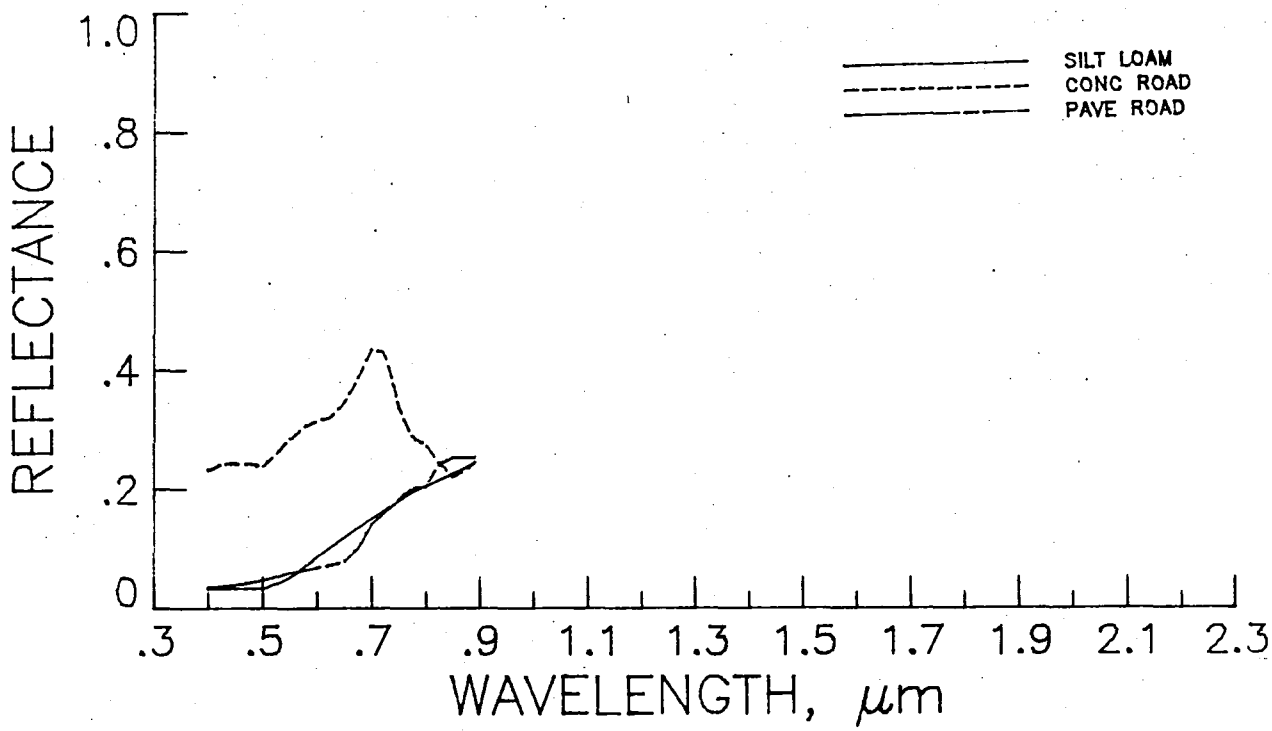

FIGURE 3.9 SPECTRAL REFLECTANCES

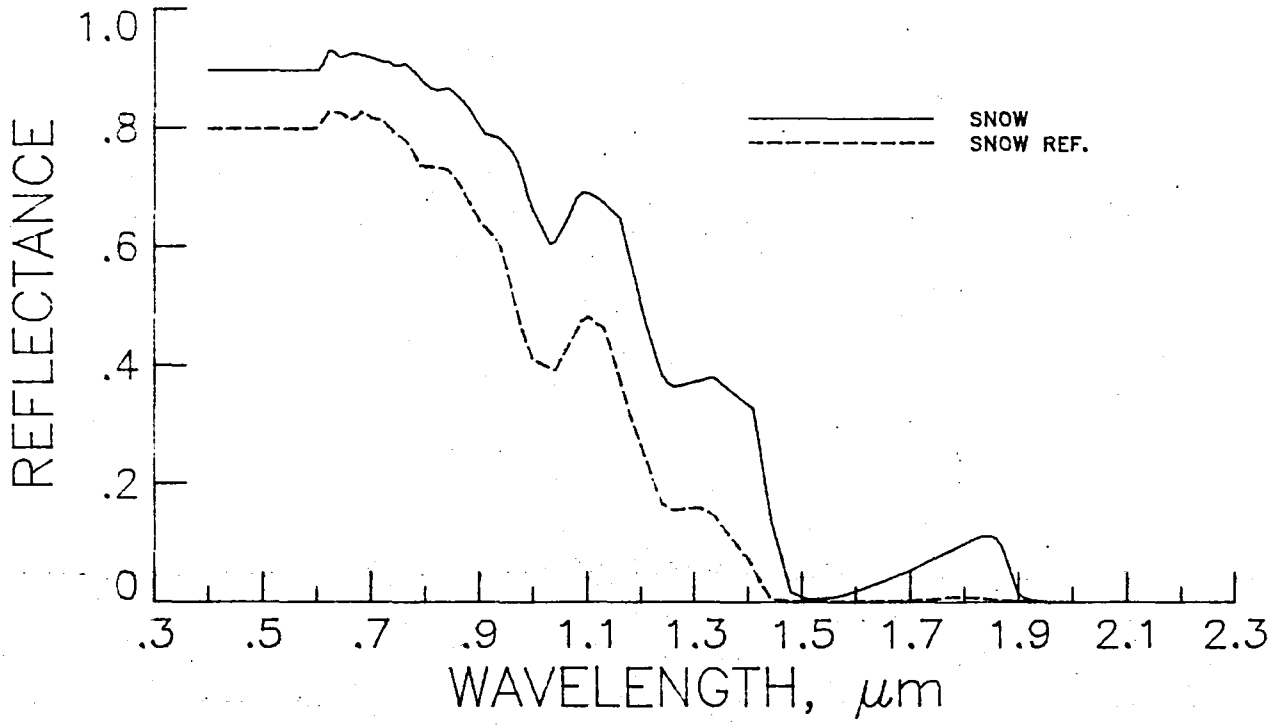

FIGURE 3.10 SPECTRAL REFLECTANCES

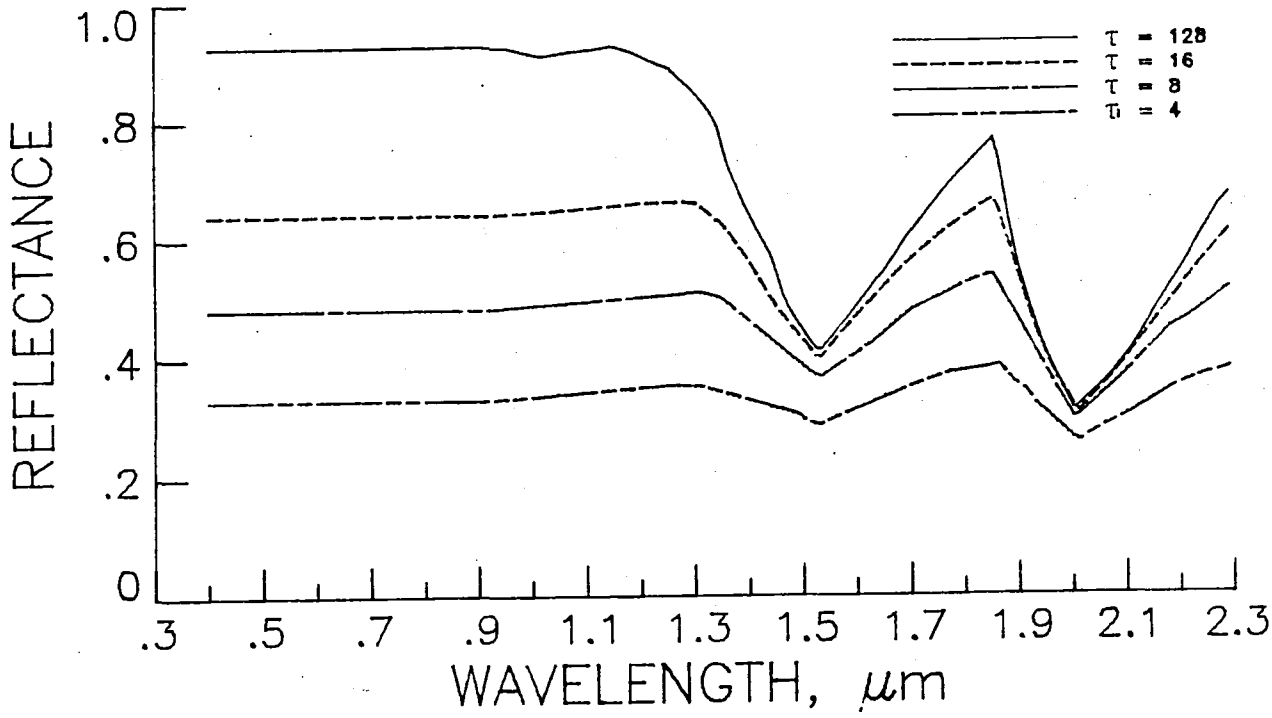

FIGURE 3.11 SPECTRAL REFLECTANCES (τ = OPTICAL THICKNESS)

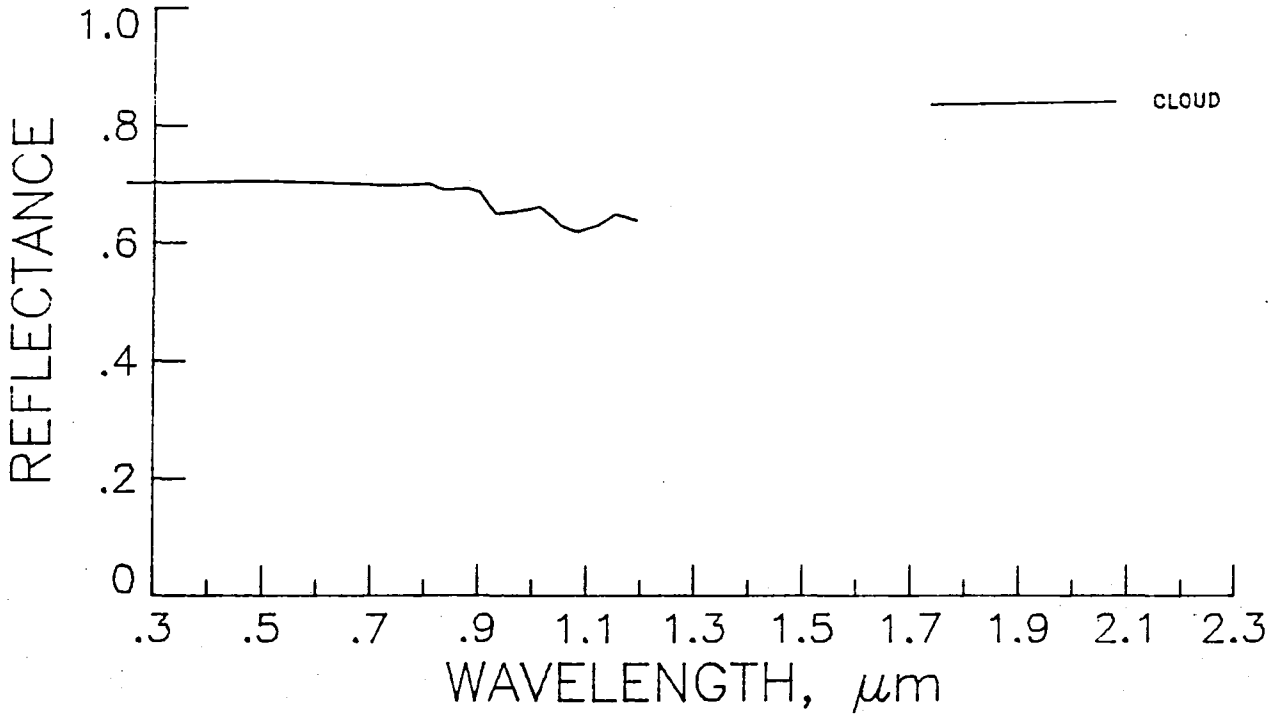

FIGURE 3.12 SPECTRAL REFLECTANCE

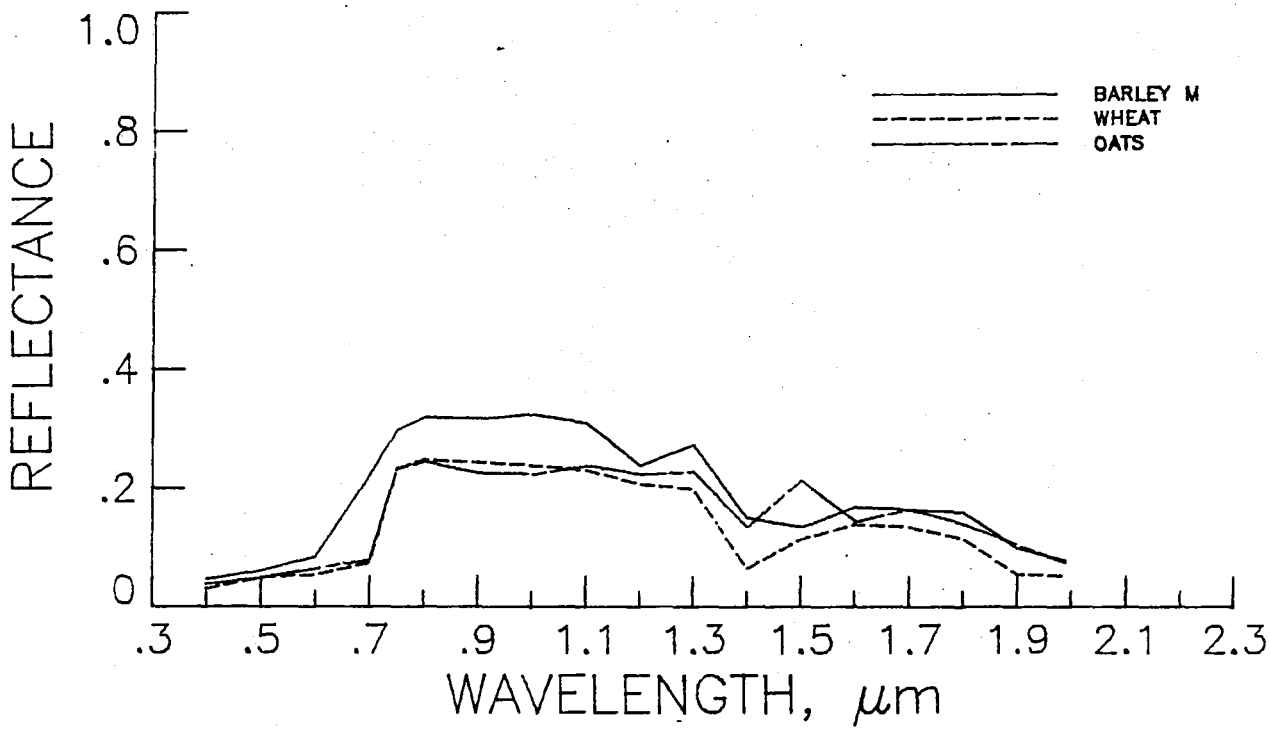

FIGURE 3.13 SPECTRAL REFLECTANCES

4. CLOUD DETECTION

4.1 Background

For an Earth resource observation system clouds present a major limitation to the collection of data. Worldwide cloud cover is approximately 45% (Barnes et al., 1968), which represents a very significant potential for obscuration of ground targets. The ability to indentify clouds reliably would allow several options for smart sensor systems including the ability to avoid imaging of cloudy areas and to eliminate cloud pixels from the data to be transmitted to ground stations. An even more sophisticated task for a sensor system with reliable cloud detection capability would be the selection of alternate imaging areas in the event that the primary target is cloud covered.

In order to identify clouds they must be adequately characterized spectrally. As one can imagine, determining the spectral reflectance of a cloud is no easy task. The reflectance data available for clouds has generally been the product of radiative transfer modeling (Hansen 1969, Novoseltsev, 1965). In the visible and near-infrared region of the spectrum both snow and clouds form a single category of what might be called bright white targets. Within this spectral region the two classes have such closely similar spectral characteristics as to make the identification of clouds as a class unreliable. Only in the longer infrared wavelengths do the two classes show significant differences.

Valovcin (1978) made a important comprehensive study of the snow/cloud discrimination problem specifically aimed at potential on-board methods. Valovcin utilized, for his analysis, spectral radiance data from cummulus and cirrus clouds and snow obtained from a high flying aircraft. He analyzed several different discrimination tasks including identifying different cloud types. For the simple cloud versus snow discrimination he found that a radiance threshold for a .11 μm bandwidth spectral channel centered at 1.56 μm achieved an 85% + accuracy. Though no test results were reported for such, he suggests that moving the channel center to 1.525 μm might improve results.

4.2 Test

Based on results and data reported by Valovcin (1978) a new channel was

added to the basic set of two channels used in the target categorization tests reported in Aherron, et al. (1981). Those channels consisted of one centered at .65 μm and one centered at .85 μm with a bandwidth of .02 μm. The new channel for cloud detection was centered at 1.55 μm with a .1 μm bandwidth.

As was indicated above the reflectance data utilized in the modeling was the result of theoretical investigations. Hansen (1969) used the doubling method solution to the radiative transfer equations, discussed in the section concerning atmospheric radiative transfer, to determine the diffuse spectral reflectance of ice clouds of various optical thickness. Novolsel'tsev calculated the spectral reflectance of a cloud composed of water droplets. Zander (1966) measured the reflectance of laboratory generated ice clouds and his data compares favorably with that report by Hansen (1969). Stochastically clouds are treated the same as non-vegetated surfaces.

A cloud detection algorithm was formulated based on the 3 above channels. The algorithm is basically a two level decision tree. First, the snow/cloud category is seperated from the other categories based on a threshold radiance in the .65 μm channel. This is the method previously used in simple categorization (Aherron, et al. 1981). The second level decision of snow versus cloud is based on a threshold in the 1.55 channel. Figure 4.1 shows the covariance elipse plots for a collection of targets similar to those used in Aherron, et al. (1981) simulated for 23 km visual range. The first level categorization boundaries are indicated by dotted lines. Included in the snow/cloud category are a snow target, an optically thick water droplet cloud, and four ice clouds of various optical thicknesses. The ice clouds are indicated on the ellipse plot according to optical thickness.

The ill-placed clouds are a manifestation of two problems in dealing with clouds. First is the problem of thin clouds. It is an arbitrary decision as to what constitutes a cloud and what is merely haze in terms of the magnitude of their effect on the received signal. Secondly, the method by which clouds are simulated assumes a perfectly absorbing background (immediately behind the target as opposed to that outside the field of view). Thus clouds of low optical thickness, with a corresponding significant transmissive contribution to radiance will be simulated as having too low a radiance, by a magnitude

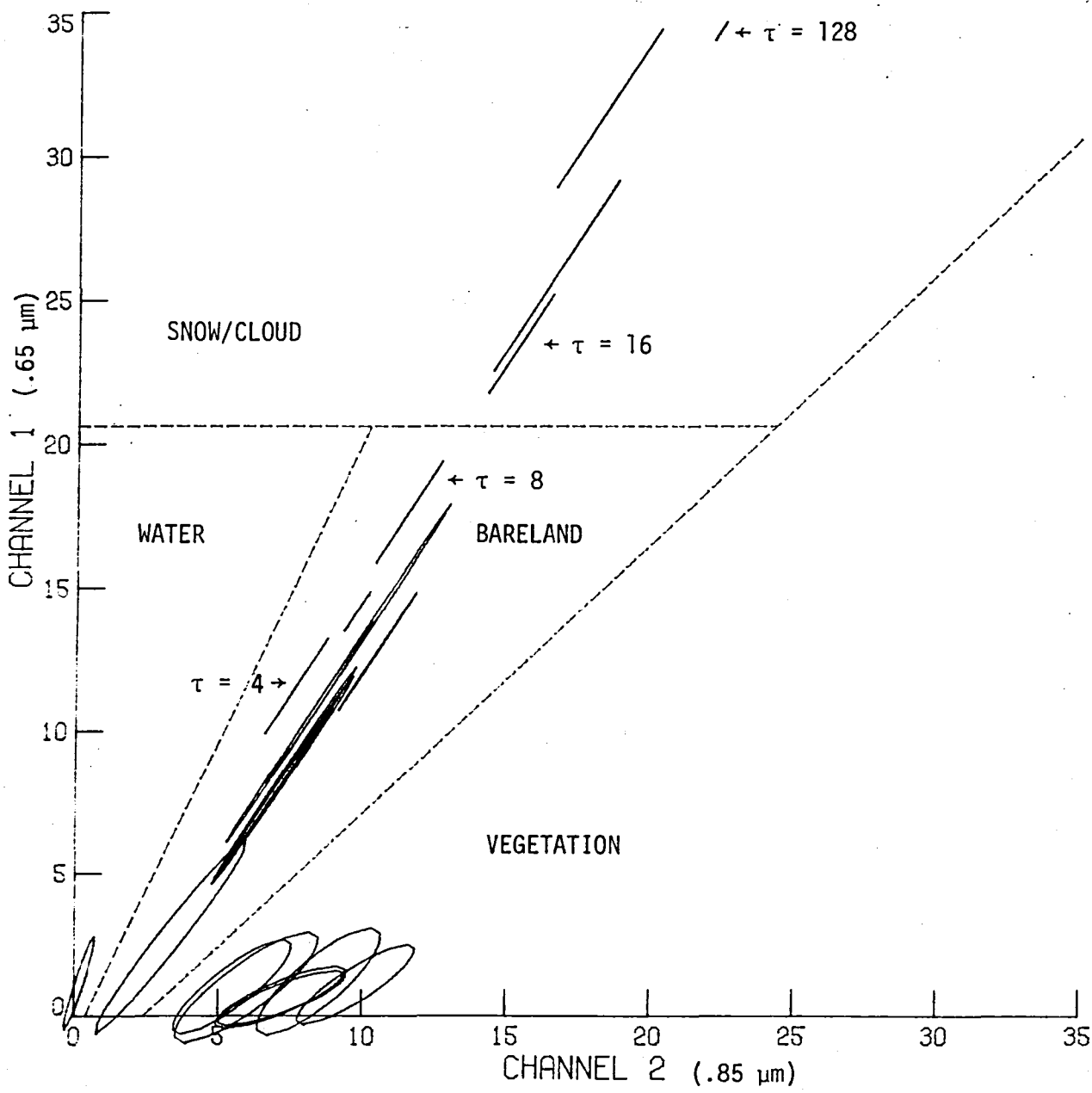

FIGURE 4.1 COVARIANCE ELLIPSE PLOT FOR 23 km VISUAL RANGE AND 30% SOLAR ZENITH ANGLE WITH ICE CLOUDS ANNOTATED WITH OPTICAL THICKNESS.

dependent on the intended background. The cloud set used to test the algorithm was limited to those with optical thickness of 16 or greater in order to make the results of snow versus cloud more meaningful. This limits the test of the ability to distinguish snow versus clouds to those pixels that can be reliably categorized as snow/clouds.

Figure 4.2 shows the .65 μm versus 1.55 μm ellipse plots for a similar but smaller set of data as used for Figure 4.1. The cloud and snow classes have been indicated. A threshold value in the 1.55 μm channel can be seen to seperate snow and clouds fairly well. This algorithm was implemented and tested for the three atmospheric conditions (as qualified by visual range), and used two solar zenith angles for testing in Aherron, et al. (1981).

Overall the snow versus cloud discrimination accuracy was very good. The worst case was for a visual range of 5 km but the difference between 5 km, 10 km, and 23 km results was insignificant. Table 4.1 shows the snow and cloud confusion matrix for the 5 km case.

The above test has served to show that given perfect snow/cloud versus other categorization the snow versus cloud discrimination is simple and accurate. In practical applications the snow/cloud versus other categorization can be rather unreliable. It will be the major source of error in dealing with clouds.

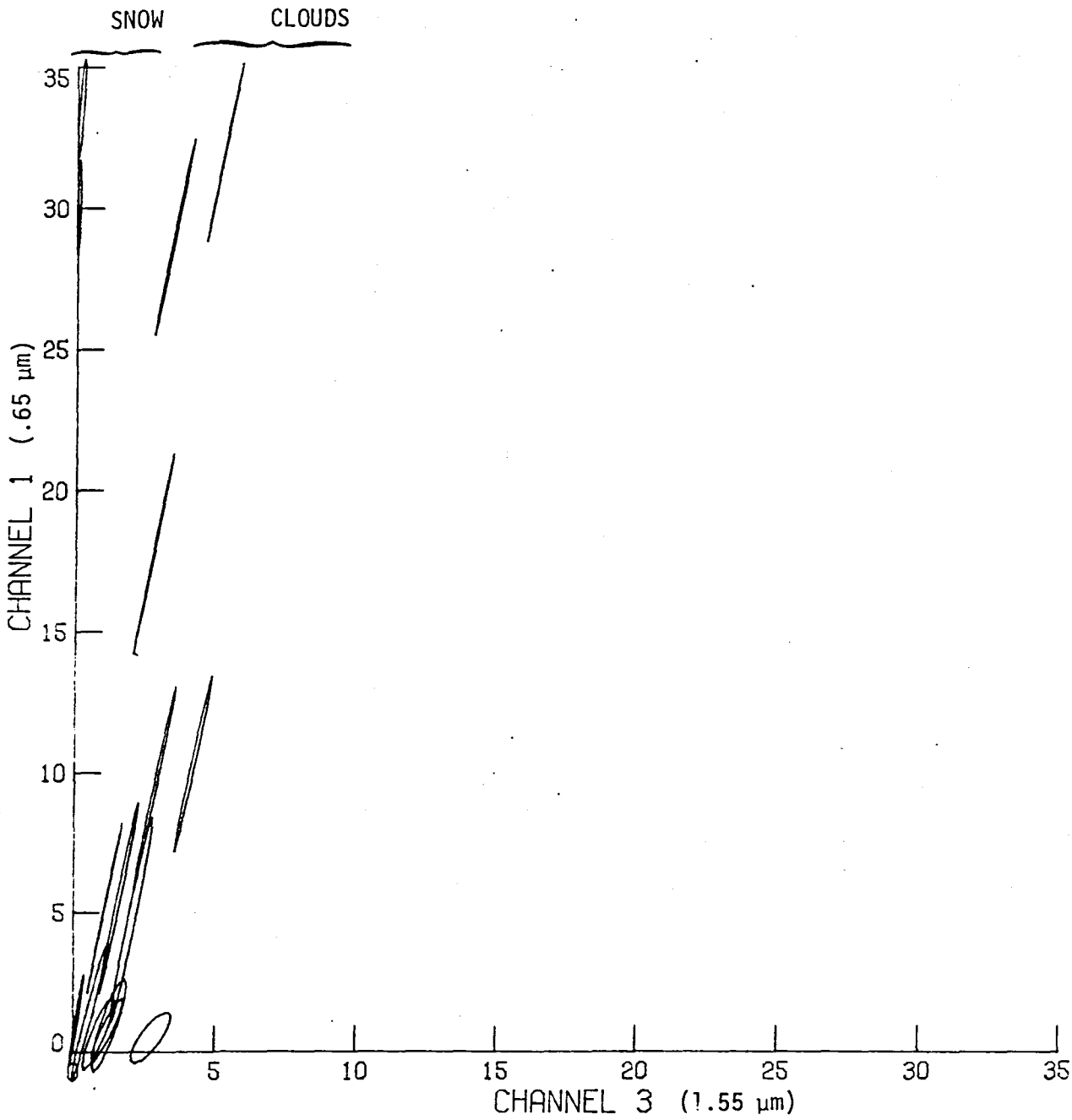

FIGURE 4.2 COVARIANCE ELLIPSE PLOT FOR 23 km VISUAL RANGE AND 30° SOLAR ZENITH ANGLE WITH SNOW AND CLOUDS INDICATED

TABLE 4.1

Snow versus Cloud confusion matrix for 5 km visual range and 30° solar zenith angle.

		DECISION	
		SNOW	CLOUD
TRUTH	SNOW	198	2
	CLOUD	0	346

5. MODEL ENHANCEMENT TESTS

Subsequent to the publication of Aherron, et al. (1981) an enhancement was made to the aerosol and Rayleigh attenuation coefficients ($\alpha i(\lambda)$) which altered the spectral radiance signatures produced by the simulation. Figure 4.1 represents signatures produced utilizing the new coefficients. Two of the three experiments in Aherron, et al. were repeated with enhanced coefficients and are summarized in Table 5.1.

Table 5.1(A), which corresponds to Figure 8(B) of Aherron, et al., shows results for the 7 class set. There are two major conclusions that can be drawn from this figure. One is that the MLH (Maximum Likelihood) aggregation method is fairly sensitive to changes in solar zenith angle. Second, recalling that the BAM (Boundary Approximation Method) is substantially cheaper computationally, the BAM is the best method of the three for the task of categorization for this set of classes.

Figure 5.1(B), which corresponds to Figure 8(C) of Aherron, et al., shows results for a larger set of 20 classes. Again the MLH method proves susceptable to changes in solar zenith angle. The MSD (mean square distance) aggregation method gave the highest accuracy but with the increased cost over the BAM. These new results show even more dramatically the importance of the mix of classes (i.e task assignment) in determining sensor system performance. Ultimately the mix of classes on which sensor systems are tested should be based on realistic probability of occurrence data. This final point will be elaborated on in Section 6.

TABLE 5.1 (A)

CATEGORIZATION ACCURACIES FOR 3 VISUAL RANGES AND TWO SOLAR ZENITH ANGLES FOR 17 CLASSES.

	SOLAR ZENITH ANGLE					
VISUAL RANGE	30°			40°		
	MLH	MSD	BAM	MLH	MSD	BAM
23 km	1.	.96	.99	.91	.96	.98
10	1.	.96	.99	.91	.95	.98
5	1.	.96	.99	.91	.96	.98

TABLE 5.1 (B)

CATEGORIZATION ACCURACIES FOR 3 VISUAL RANGES AND TWO SOLAR ZENITH ANGLES FOR 20 CLASSES.

	SOLAR ZENITH ANGLE					
VISUAL RANGE	30°			40°		
	MLH	MSD	BAM	MLH	MSD	BAM
23 km	.96	.93	.86	.85	.90	.86
10	.95	.91	.86	.85	.90	.86
5	.96	.92	.87	.85	.91	.86

ALL TRAINING SETS GENERATED FOR 23 km VISUAL RANGE AND 30° SOLAR ZENITH ANGLE.

6. STOCHASTIC MODELING

6.1 Introduction

This section deals with the stochastic nature of the remote sensing system simulation. The analytical details of the stochstic properties of the model have been discussed in other sections or in other papers (Huck, et al., 1982). Included in this section are observations and discussions concerning the limitations encountered and the implications of various assumptions made in the treatment of stochastic model properties.

The general philosophy in addressing the statistical properties of the remote sensing system has been to statistically characterize the fundamental values or processes within each model element. For instance, during the discussion of atmospheric radiative transfer models, it was stated that it was the amount and characteristics of the atmospheric constituents that was "driving" variation in radiance quantities. The limit of resolution to which this fundamental characterization is carried is defined by practical realization, as opposed to availability considerations. For plants it is realistic to collect statistical data on biomass for good size data sets. It is unrealistic to expect statistical data on the number of leaves and their orientation, twig volume, and number of flowers or fruits for anything but a small collection of cases. Due to the scarcity of good statistical data on target characteristics (i.e., biomass, water content) reflectance variability was driven by an artifical variable. Statistical data at the process resolution desired was not always available or complete and estimates were used where necessary. For targets, statistical data was not available for the fundamental characteristics or for the reflectances.

6.2 Statistical Distribution Characteristics

The assumption of the normality of statistical distriubtions in remote sensing work is almost universal. For those quantities, such as sensor irradiance, which are a function of many independently (perhaps) distributed quantities, the central limit theory of statistics would provide some justification for that assumption.

Strictly speaking, the normal distribution is not valid for quantities such as path radiance because of the exclusion of negative radiances. The normal distriubtion was chosen for the distribution of the atmospheric constituent amounts and reflectance artificial variables. For atmospheric constituent amounts this assumption is intuitively pleasing. The case of reflectance variables does not offer such appeal. One problem concerns the rather arbitrary nature by which targets are identified. For instance, one may ask at what point does thin vegetation become bare land or what is the difference between a thin cloud and thick haze. If for example, the reflectance variable for vegetation were biomass, there seems no intuitive justification for assuming that it is normally distributed. A more likely case would be an asymmetrical distribution that peaked at the biomass deemed to be the necessary minimum to be classified vegetation. The second major limitation with regards to reflectance artificial variables is the restriction of reflectance to the range of 0 to 1. For a particular portion of the spectral reflectance curve for a target characterized by low or high mean reflectance, the range of possible reflectances is truncated. If the normal assumption is used for the artificial variable in this situation, the allowable size of the reflectance variability is unduly restricted.

The failure of the normal assumption for radiance data has been demonstarted both in field and computational experiments. Valovcin (1978) plotted mean radiance and ±1 sigma radiance curves for snow and cirrus clouds. Both of the minus sigma curves showed radiances below zero which are physically impossible. Presenting ± sigma curves (or bars) suggests things about the statistical distribution that may or may not be true. Sigma curves, which are symmetric about the mean, lead the reader to believe that the probability density function (PDF) is symmetrical. The plots presented by Valovcin clearly preclude the assumption of a symmetrical PDF and therefore rule out the normal assumption. Similarily the 1 sigma ellipses for several simulated classes in Fig. 4.1 enclose negative radiances in the same manner as Valovcin's data.

6.3 Distribution Parameters

It was mentioned briefly in the section on reflectance there is a correspondence on covariance between channels and their redundancy. The exact redundancy is a function of the probability density functions of the channels.

For a multivariate normal distribution the channel redundancy is specified exactly by the covariance matrix (see for example a text on Information Theory) and this is the distribution that will be assumed for illustrative purposes. Using the same normality assumption, Wiersma and Landgrebe (1979) attributed all the covariance for a set of spectral radiance data to covarying reflectances, with one exception. The atmospheric water vapor absorption bands were eliminated from the analysis. The sophistication and rigor of their analysis is almost unparalled in the remote sensing literature, and should be reviewed to understand the importance of covariance "structure" in determining optimal spectral channels. One of the shortcomings of Wiersma and Landgrebe's analysis is the lack of consideration given to the contribution of the atmospheric variability to the spectral radiance covariance structure. This shortcoming is almost certainly due to the lack of data to quantify and statistically characterize the atmospheric effects present in the data.

The simulation that has been discussed herein has the capability to combine the effects of the reflectance and the atmosphere on the spectral radiance covariance structure. The reflectance covariance structure was discussed in the surface reflectance section. Defining the atmospheric contribution to radiance covariance has been no more fruitful than for the reflectance. The model utilized for atmospheric radiative transfer variability requires that the covariance of atmospheric constituent amounts be defined. For example, it would be necessary to define the correlation between atmospheric water vapor content and aerosol burden. So far no such data has been found. Simulations run to date have assumed all constituents to be uncorrelated with the exception of aerosols and water vapor which are assumed to have perfect positive correlation. Fraser (1975) reports covariance data for optical depths determined from solar attenuation data. By assuming some model for the various atmospheric constituents contributions to optical depth, it might be possible to invert the covariance data for the constituent amounts but so far efforts in this area have not been successful.

6.4 Decision Theory Considerations

It became apparent during the work represented in Aherron, et al. (1981) and cloud detection algorithm performance reported herein that classification

or categorization accuracies where highly dependent on the probability of encountering various targets. This is a familiar subject to those with knowledge of Bayesian decision theory. The two statistical values necessary for Bayesian decision calculations are the conditional probability of a signal given that it was produced by a certain class and the a priori probability of encountering that class (Duda and Hart, 1973). The statistical characterizations and models discussed to date have been concerned with defining the conditional probability function for a class. The algorithm performance evaluation model utilized thus far has been a simple overall classification or categorization accuracy. These figures have been based on equal a priori probabilities for classes. When classes are aggregated into categories the a priori probabilities are not necessary equal. This point must be kept in mind when comparing the reported overall decision accuracies.

Discussion of the Boundary Approximation Method (BAM) decision algorithm in Aherron, et al. (1981) points out the need for class a priori probabilities in balancing the type I and type II errors of categorization when formulating the exact algorithm parameters. As the overall remote sensing model becomes more realistic and accurate in future work, it will be necessary to include realistic a priori probabilities of occurence for both classes and categories. At least two potential methods for channel bandwidth and location selection will require such knowledge. One of these, an information theory based method, was used by Kondratyev (1975) for choosing spectral channels. Kondratyev's analysis was fairly crude and the method he used is still relatively unexplored. Secondly, Bayesian Decision Theory, as was discussed before, requires the same class probability data.

7. SUMMARY & CONCLUDING REMARKS

This report has presented supporting research and data for a previously reported comprehensive remote sensing system simulation (Huck, et al. 1982). A review of various models of atmospheric radiative transfer was presented. The qualitative accuracy and the quantitive computational complexity of the various models was compared. Using those comparisons and evaluation criteria that included recognition of the uncertainties about atmospheric parameters, the Turner (1974) model was chosen for use in the remote sensing system simulations. A detailed discussion of the stochastic implementation of the Turner model was given. Various functional forms for spectral diffuse reflectance that allow introduction of variability were given and discussion was made of certain properties of reflectance variability that are desirable in dealing with realistic targets. A compilation of various spectral reflectance curves utilized in simulations was presented.

The special problem of detecting clouds reliably has been examined. For optically thick clouds a test of a preliminary detection algorithm has shown very high accuracy. Thin clouds pose a problem in detection that needs to be examined more closely. The detection algorithm tested requires a spectral channel at .65 μm and 1.55 μm. As was pointed out in Huck, et al., (1982), the remote sensing system simulation being developed is unique in its treatment of the stochastic elements of the remote sensing system. The lack of good data for parameterizing the statistical nature of the atmosphere and target reflectances was discussed especially as it pertained to defining the wavelength covariance matrix for radiances. The need for a priori probability of occurence data for targets was discussed. Finally, a partially updated set of categorization results for the experiment reported in Aherron, et al. (1981) was presented which showed the simplest method of categorization performing even better relative to the other methods than previously reported.

Hopefully modeling efforts such as described provide insight to the overall sensor systems design effort as well as those people involved in basic research concerning fundamental processes.

One role that remote sensing system modeling plays in research is to encourage a more insightful look at available data and more careful definition of needs for future data collection. Specifically the statistical nature

of the various system elements becomes more important as the modeling becomes more refined and generalized. And finally, modeling should help to make informed decisions as to the importance of various effects and error sources within remote sensing systems.

8. REFERENCES

Aherron, R.M.; Arduini, R.F.; Davis, R.E.; Huck, F.O.; and Park, S.K., (1982) Earth Feature Identification for Onboard Multispectral Data-Editing: Computational Experiments, Proc. Conference on Optical Information Processing for Aerospace Applications, NASA CR-2207, pp. 17-32.

Barbe, D.F., Ed. SMART Sensors, Proceedings of the Society of Photo-Optical Instrumentation Engineers, Vol. 178.

Barnes, J.C.; Glasen, A.H.; Sherr, P.E.; and Willand, J.H., (1968) World-Wide Cloud Cover Distribution for Use in Computer Simulations Final Report, Allied Research Assoc., Inc., Concord, Mass., NASA CR-61226.

Bowers, S.A.; and Hanks, R.J., (1965) Reflection of Radiant Energy from soils, Soil Science 100:130-138.

Breckenrideg, R.A.; Ed. (1979) Remote Sensing of Earth From Space: Role of "SMART Sensor", Progress in Astonautics and Aeronautics, Vol. 67.

Collins, W., (1978) Remote Sensing of Crop Tree and Maturity. Photogrammetric Engineering and Remote Sensing, 44(1):43-55.

Condit, H.R., (1970) The Spectral Reflectance of American Soils. Photogrammertric Engineering, 36(9):955-966.

Dave, J.V., and Canosa, J., (1974) A Direct Solution of the Radiative Transfer Equation: Application to Atmospheric Models with Arbitrary Vertical Non-homogeneitics, J. Atmospheric Sciences, 31:1089-1101.

Dave J.V., (1978) Extensive Data Sets of the Diffuse Radiation in Realistic Atmospheric Models with Aerosols and Common Absorbing Gases, Solar Energy, 21:361-369.

Dave, J.V., (1979), Contrast Attenuation Factors for Remote Sensing, IBM Journal of Research and Development, 23:214-224.

Duda, R.O.; and Hart, P.E., (1973) Pattern Classification and Scene Analysis., John Wiley and Sons, New York.

Duggin, M.J., (1974) On the Natural Limitation of Target Differentiation by Means of Spectral Discrimination Techniques. Proceedings of the Ninth International Symposium on Remote Sensing of the Environment.

Fraser, R.S., (1975) Degree of Interdependence Among Atmospheric Optical Thickness in Spectral Bands Between 0.36-2.4 um. J. Applied Meteorology, 14(6): 1187-1196.

Hansen, J.E., (1969) Radiative Transfer by Doubling Very Thin Layers, Astrophysical Journal 155:565-573.

Horvath, R.; Spencer, M.; and Turner, R. (1972) Atmospheric Correction and Simulation of Space acquired Remote Sensor data: 4 to 1.0 um Spectral Range, NASA CR-152922, WRL-10567050F.

Kiang, R.K., (1981) The Atmospheric Influence on TM Measurements and its Comparison with the Influence on MSS Digest of the Int. Geoscience and Remote Sensing Symposium, IEEE CAT. 81CH1656-8:826-833.

Kondratyev, K.Ya.; Grigor ev, AL. A.; and Pokraovskiy, O.M., (1975) Information Content of the Data Obtained by Remote Sensing of the Parameters of the Environment and the Earth's Resources from Space, Izdatel'stvo Leningradskogo Universiteta, NASA TT F-16435.

Krook, M., (1955) on Solutions of the Equations of Transfer, Astrophysical Journal, 122(3):488-497.

Lampley, C.M.; and Blattner, W.G.M., (1978) E-O Sensor Signal Recognition Simulation: Computer Code SPOT I, Radiation Research Associates, Fort Worth, Texas, Report RRA-T7809, pp. 108.

Leeman, V.; Earing, D.; Vincent, R.K.; and Ladd,S., (1971) The NASA Earth Resources Spectral Information System: A Data Compilation. NASA CR-115757.

Liou, K.N., (1973) A Numerical Experiment on Chandrasekhar's Discrete-Ordinate Method for Radiative Transfer: Applications to Cloudy and Hazy Atmosphere, J. Atmospheres, J. Atmospheric Sciences 30(7):1303-1326.

Liou, K.N. (1980) An Introduction to Atmospheric Radiation, Academic Press, New York.

Liou, K.N., (1974) Analytic Two-stream and Four-stream Solutions for Radiative Transfer, J. Atmospheric Sciences, 31: 1473-1475.

Liou, K.N., (1975) Applications of the Discrete-Ordinate Method for Radiative Transfer to Inhomogeneous Aerosol Atmosphere, J. Geophysical Research, 80(24): 3434-3440.

Malila, W.A.; Crane, R.B.; Omarzu, C.A.; and Turner, R.E., (1971) Studies of Spectral Discrimination, NASA CR-134181, WRL 31650-22-T.

Maxwell, E.L., (1976) Multivariate System Analysis of Multispectral Imagery, Photogrammetric Engineering and Remote Sensing, 42(9):1173-1186.

Novosel'tsev, Ye.P., (1965) Spectral Reflectivity of Clouds, NASA TT F-328.

O'Brien, H.W.; and Munis, R.H., (1975) Read and Near-Infrared Reflectance of Snow. U.S. Army Cold Regions Research and Engineering Laboratory Research Report 332 (ADA007732).

O'Neill, N.T.; and Miller, J.R., (1977) Comparison of Two Methods to Determine the Path Radiance Observed From Above the Atmosphere, 4th Canadian Symposium on Remote Sensing, pp. 573-582.

O'Neill, N.T.; Miller, J.R.; and Ahern, F.J., (1978) Radiative Transfer Calculations for Remote Sensing Applications, Proc. 5th Canadian Symp. on Remote Sensing, pp. 572-578.

Orr, D.G.; Dworknik, S.E.; and Young, L.M. (1963) Reflectance Curves of Soil, Rocks, Vegetation, and Pavement. Research Report 1746-RR, U.S. Army Engineer Reseach and Development Laboratories, Fort Belvoir, VA.

Otterman, J.; Undar, S.; Kaufman, Y.; and Podolak, M., (1980) Atmospheric Effects on Radiometric Imaging From Satellites Under Low Optical Thickness Conditions, Remote Sensing of Enviornment. 7: 115-129.

Park, S.K.; Davis, R.E.; Huck, F.O.; and Arduini, R.F., (1980) Multispectral Data Acquisition and Classification: Computer Modeling for SMART Sensor Design, Proc. AIAA Sensor Systems for the 80's Conference.

Park, J.K.; and Deering, D.W., (1981) Relationships between Diffuse Reflectance and Vegetation Canopy Variables Based on the Radiative Transfer Theory. Techn. Paper ASP-ACSM Convention, Washington, DC.

Roa, V.T.; Branch, E.J.; and Mack, A.R., (1978) Crop Discriminability in the Visible and Near Infrared Regions, Photogrammetric Engineering and Remote Sensing, 44(9): 1179-1184.

Ronnholm, K.; Baker, M.B.; and Harrison, H., (1980) Radiative Transfer through Media with Uncertain or Variable Parameters, 37: 1279-1290.

Slater, P.N., (1980) Remote Sensing, Optics and Optical Systems. Addison-Wesley Publ. Co., London.

Selby, J.E.A.; Kneizys, F.X.; Chetwynd, J.H,M Jr,; and McClatchey, R.A. (1978) Atmpsoheric Transmittance/Radiance: Computer Code LOWTRAN4. AFSL-TR-78-0053, Environmental Research Papers, No. 626. Zander, R., (1 9966), Spectral Scattering Properties of Ice Clouds and Hoarfrost. Journal of Geophysical Research, 71(2): 375-378.

Smith, J.A.; and Ranson, K.J., (1979) Multispectral Resources Sampler "Proof of Concept" Literature Survey of Bidirectional Reflectance, ORI, Inc., Silver Springs, MD.

Suits, G.H.; and Safir, G.R., (1972) Verification of a Reflectance Model for Mature Corn with Applications to Corn Blight Detection. Remote Sensing of Environment, 2:183-192.

Tucker, C.J., (1977) Asymptotic Nature of Grass Canopy Spectral Reflectance, Applied Optics, 16(5): 1151-1156.

Tucker, C.J.; and Maxwell, E.L., (1976) Sensor Design for Monitoring Vegetation Canopies, Photogrammetric Engineering and Remote Sensing, 42(11): 1139-1410.

Turner, R.E. (1974) Radiative Transfer in Real Atmospheres, NASA CR-ERIM 190100-24-T.

Valovcin, F.R., (1978), Spectral Radiance of Snow and Clouds in the Near Infrared Spectral Region. AFGL-RE-78-0289, Air Force Surveys in Geophysics, No. 403.

Vicek, J., (1974) Difficulties in Determining Meaningful Spectral Signatures of Forest Tree Canopies. Proceedings of Sympsium on Remote Sensing and Photo Interpretation, International Society for Photogrammetry, Alberta, Canada.

Wiersma, D.J.; and Landgrebe, D.A., (1979) An Analytical Approach to the Design of Spectral Measurements in the Design of Multispectral Sensor, IEEE Machine Processing of Remotely Sensed Data Symposium.

Wolfe, W.L.: and Zissis, G.J., (1978) The infrared Handbook. Environmental Research Institute of Michigan.

Zander, R., (1966) Spectral Scattering Properties of Ice Clouds and Hoarfrost. Journal of Geophys. Res., 71(2).

1. Report No.	2. Government Accession No.	3. Recipient's Catalog No.
NASA CR-165974		

4. Title and Subtitle	5. Report Date
COMPUTATIONAL MODELING OF MULTISPECTRAL REMOTE SENSING SYSTEMS: BACKGROUND INVESTIGATIONS	August 1982
	6. Performing Organization Code
7. Author(s)	8. Performing Organization Report No.
R. Martin Aherron	
	10. Work Unit No.
9. Performing Organization Name and Address	11. Contract or Grant No.
Information & Control Systems, Incorporated 28 Research Drive Hampton, VA 23666	NAS1-16367
	13. Type of Report and Period Covered
12. Sponsoring Agency Name and Address	Contractor Report
National Aeronautics and Space Administration Washington, DC 20546	14. Sponsoring Agency Code

15. Supplementary Notes

Langley Technical Monitor: Mr. F. O. Huck

16. Abstract

A computational model of the deterministic and stochastic process of remote sensing has been developed based upon the results of the investigations presented. The model is used in studying concepts for improving worldwide environment and resource monitoring. A review of various atmospheric radiative transfer models is presented as well as details of the selected model. Functional forms for spectral diffuse reflectance with variability introduced are also presented. A cloud detection algorithm and the stochastic nature of remote sensing data with its implications are considered.

17. Key Words (Suggested by Author(s))	18. Distribution Statement
multispectral band scanner, remote sensors, spectral bands, computer programs, atmospheric effects, spectral reflectance, remote sensing systems	Unclassified-Unlimited Subject Category 35

19. Security Classif. (of this report)	20. Security Classif. (of this page)	21. No. of Pages	22. Price*
Unclassified	Unclassified	52	A04

End of Document